LOW TEMPERATURE PREPARATION OF WIDE BAND-GAP METAL OXIDE THIN FILMS WITH NOVEL DESIGNED SOLUTION PROCESSES

A Dissertation

Presented to the Faculty of the Graduate School

of Cornell University

In Partial Fulfillment of the Requirements for the Degree of

Doctor of Philosophy

by

Chung-Han Wu

May 2011

LOW TEMPERATURE PREPARATION OF WIDE BAND-GAP METAL OXIDE THIN FILMS WITH NOVEL DESIGNED SOLUTION PROCESSES

Chung-Han Wu, Ph. D.

Cornell University 2011

Highly homogeneous crystalline TiO_2 thin films were prepared by spin-coating a TiO_2 nanoparticle aqueous dispersion at room temperature without further heat treatment. Using these films as electron transporting layers, inverted structure hybrid photovoltaic cells (TiO_2/P3HT) and light-emitting diodes (TiO_2/F8BT) were demonstrated. The performance of these devices show that a properly designed nanoparticle casting route can help avoid high temperature crystallization or sintering steps for TiO_2 thin films, paving the road for their use in conjunction with plastic substrates. Post-annealing of TiO_2/F8BT copolymer bilayer could remove the adsorbed hydroxyl groups in the bottom TiO_2 while also made the F8BT copolymer diffuse into the TiO_2 layer. Bulk heterojunction of electron-transporting TiO_2 and light-emitting polymer was formed after post-annealing and the performance of TiO_2/F8BT copolymer hybrid LEDs was largely improved. TiO_2/F8BT hybrid LEDs show a promising brightness ~ 7000 cd/m^2 and an outstanding current efficiency as high as 2 cd/A, which is three times higher than the efficiency of hybrid LEDs without the post-annealing treatment. MOD processed a-IGZO transistors have the basic characteristics of thin film transistors. The performance of a-IGZO TFT with the mobility of 3.4 $cm^2V^{-1}s^{-1}$ shows the newly developed approach promising. The spin-coating preparation of a-IGZO film is a rather simple process for transistor fabrication and therefore provides the possibility of low-cost manufacture of transparent TFTs with good performance.

BIOGRAPHICAL SKETCH

Chung-Han Wu was born in Taipei City, Taiwan in 1977. He received a BS and MS in Chemical Engineering from National Taiwan University (NTU). The major projects of his undergraduate and graduate study in NTU were about ceramic materials, including sintering behavior of ceramics and the deposition of inorganic thin films. After graduating from NTU, he joined Chung Shan Institute of Science and Technology (CSIST) in 2001 as an assistant researcher studying battery and other energy related materials. During this time, he became deeply interested in advanced energy research that made him decide to pursue a Ph. D. at Cornell University. He was honored to be the first winner of Taiwan Merit Scholarship in the field of energy technology. He entered the Materials Science and Engineering program at Cornell in 2006. Under the supervision of Prof. George Malliaras, he worked on inorganic/polymer hybrid device technologies with the goal of achieving low-cost and large-scale fabrication of advanced optoelectronics. Upon graduation in 2011, Chung-Han will continue his research in renewable energy technologies as well as the development in energy industry for life.

ACKNOWLEDGMENTS

First and foremost, I would like to thank my family for their emotional support, giving me strength to keep on persevering whenever the going gets tough, especially my wife Kuei-Huei, who is always by my side and encourages me in these years. I acknowledge financial support from Taiwan Merits Scholarship. Thanks are due to my mentor – Professor Chung-Hsin Lu, who advised me with my graduate study in National Taiwan University. My research work would not have been possible without the kind assistance of the tool managers at the Cornell NanoScale Science & Technology Facility (CNF), Cornell Center for Materials Research (CCMR), and the KAUST-Cornell Center for Energy and Sustainability (KAUST-CU). I am particularly indebted to Maura Weathers, Jon Shu, and David Jung. I am grateful for the assistance of various Cornell undergraduates, Caroline Greenwood and Ashish Banerjee, who helped to fabricate and test solar cell devices as well as to synthesize the nanosized oxide particles. I am very fortunate to have enjoyed much fruitful collaboration with my talented colleagues at Cornell, Matthew Lloyd, John DeFranco, Yee-Fun Lim, Vladimir Pozdin, Alexander Zakhidov, Hon Hang Fong, Haitao Zhang, Hanying Li and Professor Lara Estroff. My committee members, Professor Paulette Clancy, Emmanuel Giannelis, and Richard Robinson have given me much valuable guidance and advice. Finally, I owe much to George Malliaras for his unwavering support and belief in me, and for giving me such an invaluable graduate school learning experience.

TABLE OF CONTENTS

CHAPTER 1

INTRODUCTION

1.1 Research motivation

- Challenge in large scale fabrication of organic electronics

Organic electronics have attracted substantial interest from the industry for their wide range of properties, such as high solubility of organic materials in solvents and the color of light emission that can be finely tuned via chemical synthesis. Another attractive feature involves processing. Coatings of organic materials with liquid processes can be easily applied over large areas and to a variety of substrates. Thus, with the ease of processing, organic electronics are considered to be promising for their low-cost fabrication.

However, device stability is still a challenging problem that limits large-scale manufacturing of organic electronics. This limitation originates primarily due to the stability of the electron transporting materials and cathode layer. First, commonly used electron transporting materials such as hydroxyquinoline based metal chelates are sensitive to the exposure to moisture and oxygen or UV radiation [1,2]. Second, low work function metals or their halides, what are usually required to improve electron injection from the cathode, can easily decompose and degrade. Therefore, vigorous encapsulation is usually required for present organic device fabrication [3]. As yet, research on the development of stable electron transporting materials for organic electronics is highly desirable. Unambiguously, metal oxides are promising candidates as electron transporters due to their superior air stability and much lower material cost for large-scale synthesis.

1.2 Technologies for the preparation of metal oxide thin films

In the industry, there are several kinds of technologies used to prepared metal oxide thin films with various conditions. Four generally used thin film preparation processes: oxidation, chemical vapor deposition, sputtering, and chemical solution deposition are briefly introduced below.

(1) Oxidation process:

There are two kinds of oxidation processes— anode oxidation and thermal oxidation process. Anode oxidation process is to set metal substrates into electrolyte and then to oxidize the metal at the anode. The control of film thickness could be precise just by the combined computation of current density and reaction time. The advantages of anode oxidation are the room temperature operation and the accurate control of film thickness. However, this process has the shortcoming that the purity of electrolyte seriously influences the thin film quality and also it is hard to be integrated into the semiconductor manufacturing process. Thermal oxidation process simply locates metal in oxygen atmosphere and oxidizes it with high temperature. The application of rapid thermal annealing (RTA) makes the soaking time of annealing shorten. The advantage of thermal oxidation is the good uniformity of product quality, but the imperfection of this process is the degradation or diffusion problem of the interface reaction between functional layers due to the high temperature annealing.

(2) Chemical vapor deposition (CVD):

This process utilizes flowing gas to bring reactants into the reactor locating objective substrates for the deposition of oxide thin films. The CVD process is made up of various elementary steps, such as the transport of reactants, adsorption, desorption and surface reaction. The volatility and thermal stability are fundamental properties of a chemical to be used as a CVD source. The CVD chemicals should be

readily volatile below temperatures at which their thermal decompositions occur. Among several precursors, low boiling point metal-organics and O_2 precursors have been usually employed for the CVD growth of metal oxide films [4,5].

CVD has the unique advantage of good step coverage while the step coverage capability is a very important factor for thin capacitor films in the three-dimensional memory cell. Further, CVD has good film thickness controllability and good uniformity of deposited films. Moreover, the facility for the formation of multiple layer or composite oxide films is also desirable for the CVD process. Nevertheless, there are still some drawbacks of the CVD process: the carbon residues in oxide films that cause leakage current, the toxicity of reactants, and the relative high reaction temperature (the deposition temperatures of CVD process are varied from 400 to 1000 ℃).

(3) Sputtering process:

The well sintered bulk of metal oxide or metal sheet is settled at the cathode and bombarded by the plasma of Ar (generally used) that generated by a glow discharge. The charged ions in the Ar plasma hit the cathode (target) surface and then induce the ejection of one or more metal atoms from the surface of the target. Finally, the ejected atoms fly through the plasma and land on the substrate that are designed for deposition. The sputtering process prevails for (1) high deposition rate, (2) the capability to maintain uniform deposition on large wafer, and (3) the absence of organic residuals. However, there are still some disadvantages: the bad control of composition for multi-elements oxide films, the poor step coverage, and the unavoidable need of vacuum environment.

(4) Chemical solution deposition (CSD):

With the metal-organic precursors or precursor solutions dissolving ionic compounds, thin films are deposited on substrates by spin-coating or dip-coating techniques, and then the films receive high temperature thermal treatment to decompose the coated reactants and crystalize the oxides. The advantages of CSD include: the stability and facilitation of process procedure and the low-cost equipment; and the easy control of composition, etc. Although the recommendations of CSD are intuitive, some imperfections still exist in this process, like the voids forming during the precursor decomposition, the contamination of residual elements C and H that induces leakage current, and the relatively high annealing temperatures.

From the description above, we know that though metal oxide films can be prepared with several special processes according to different condition requirements, it is still difficult to apply oxide thin films to the organic electronics. First, most organic materials, including the flexible plastic substrates, cannot survive after high temperature post annealing required to remove the organic residues from precursors or to crystalize the oxides. Second, in order to fabricate electronic devices with good and stable performance and reasonable lifetime, the integrated films used in electronic devices should be uniform and the impurity content inside is strictly limited. Moreover, the future of organic electronics lies in large-scale, low cost applications, thus the requirement of vacuum environment while preparing oxide films weakens the advantage of organic/oxide hybrid electronics. Thus, in order to incorporate metal oxide thin films into organic electronics, low-temperature preparation that processes in atmospheric surrounding is highly required.

1.3 Wide band-gap metal oxides

Wide band-gap oxides (generally band-gap > 3.0 eV) have been studied

intensively for their useful applications to optoelectronic devices and transparent field-effect transistors (FETs) because they are optically transparent in the whole visible region. For example, transparent conducting oxides (TCO), such as indium tin oxide (ITO) and fluorine-doped tin oxide (FTO) thin films, have been extensively incorporated as transparent electrodes in photovoltaic cells, organic light-emitting diodes (OLED), and as pixel electrodes in devices such as liquid-crystal displays (LCD). Besides TCO films, wide band-gap semiconducting oxides have also received great attention in decades for their applications to electronic devices as electron transporters or active layers in thin-film transistors (TFTs), moreover, these semiconducting oxides are promising catalysts for advanced photocatalysis reactions. Besides the good electric properties and the possibility of being transparent, the outstanding features of wide band-gap semiconducting oxides also include their excellent stability and low material costs due to the abundant content in the earth's crust and the ease of mass production. The materials in this category that attract more interest of the industry are titanium dioxide (TiO_2), zinc oxide (ZnO) and amorphous oxide semiconductors (AOSs).

1.3.1 Titanium dioxide

TiO_2 has three commonly encountered crystalline polymorphs: rutile, anatase, and brookite, and all of them are built upon the connection of six coordinated titanium (TiO_6 octahedra) in their crystal structures (**Figure 1.1**). Because of the metastability of the brookite form, the most common forms of synthetic TiO_2 crystals are rutile and anatase. The anatase structure consists of edge-sharing TiO_6 octahedra, while the rutile and the brookite frameworks exhibit both corner- and edge- sharing configurations: **(a)** In rutile structure, each TiO_6 octahedron shares two edges with other octahedrons to form chains, and these chains are then linked together via corner connection. **(b)**

Anatase has no corner sharing but has four edges shared per octahedron. As shown in the figure, the crystal structure of anatase can be viewed as kinked chains of edge-sharing octahedra, while the TiO_6 chains in rutile are linked straight. **(c)** As for brookite, the octahedra share three edges and also corners, and the dominant structural feature is a chain of edge sharing: the distorted TiO_6 octahedra are arranged parallel to the c-axis and are cross-linked by shared edges.

Rutile is considered to be the equilibrium phase at all temperatures. The anatase phase converts to rutile upon heating at high temperature [6]. Because of the high refractive index, especially the rutile phase, TiO_2 is widely used as white pigment in paints and inks. Moreover, the stability and harmlessness to human body make TiO_2 good sunscreen or UV absorber in cosmetic and skin care products.

Since 1990s, nanocrystalline titanium dioxide (TiO_2) films show a remarkable electron injection nature through the interconnection of nanoparticles [8] and are extensively used in many applications such as dye-sensitized solar cells (DSSC) [9]. Moreover, recent reports in the literature have demonstrated that OLED using a compact TiO_2 film as electron injecting bottom electrode is feasible and promising as long as the process temperatures can be decreased further [10,11].

1.3.2 Zinc oxide

ZnO is a wide band-gap oxide of the II-VI semiconductor group. ZnO crystallizes in two major forms: hexagonal wurtzite and cubic zinc blende (**Figure 1.2**), though other crystal structures may exist but they are observed only in special conditions (e.g. rocksalt structure of ZnO is observed at high pressures about 100 kbar [13]). In both wurtzite and zinc blende forms, the zinc and oxide centers are tetrahedral.

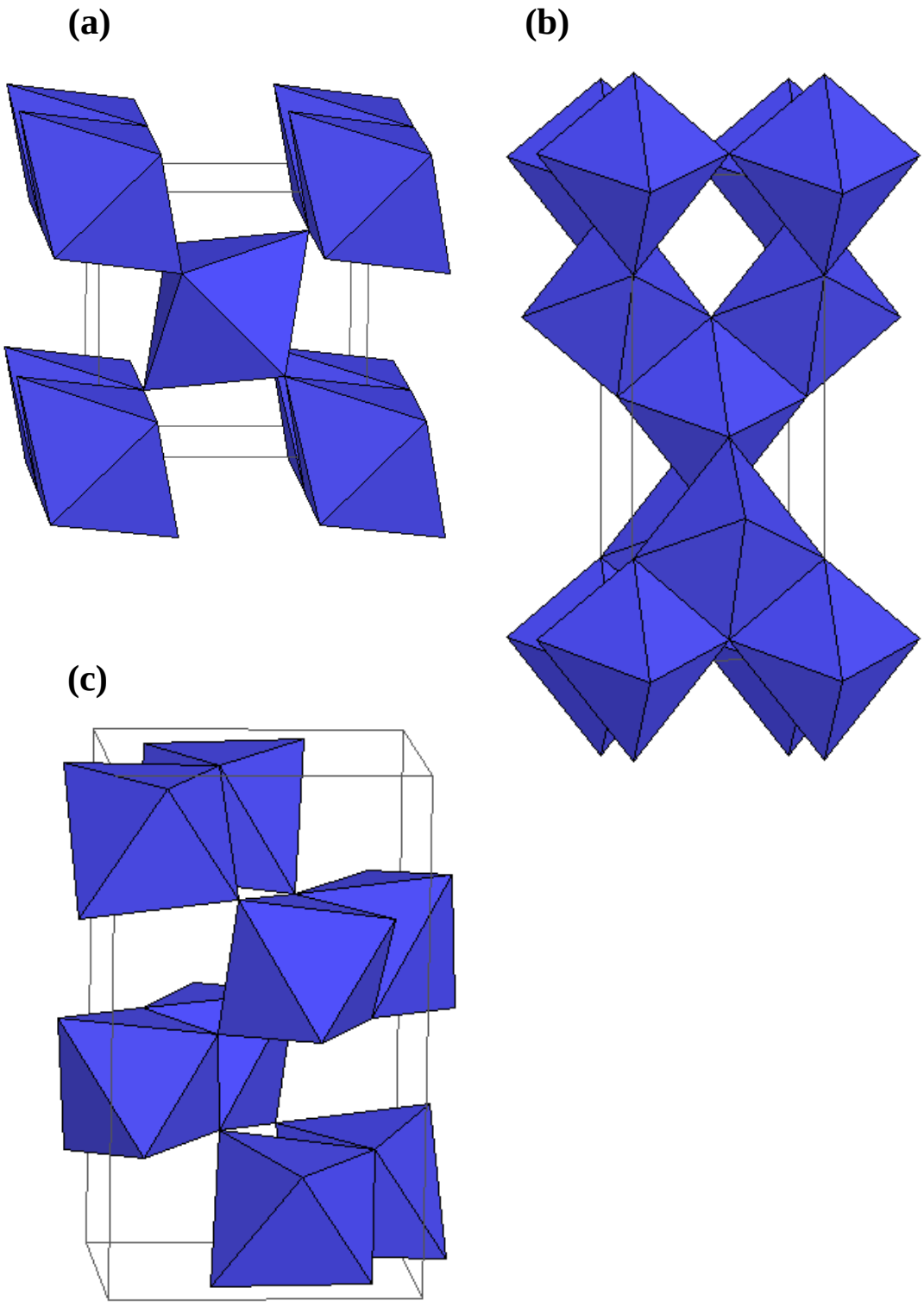

Figure 1.1 Crystal structures of TiO_2 polymorphs: **(a)** rutile, **(b)** anatase, **(c)** brookite. [7]

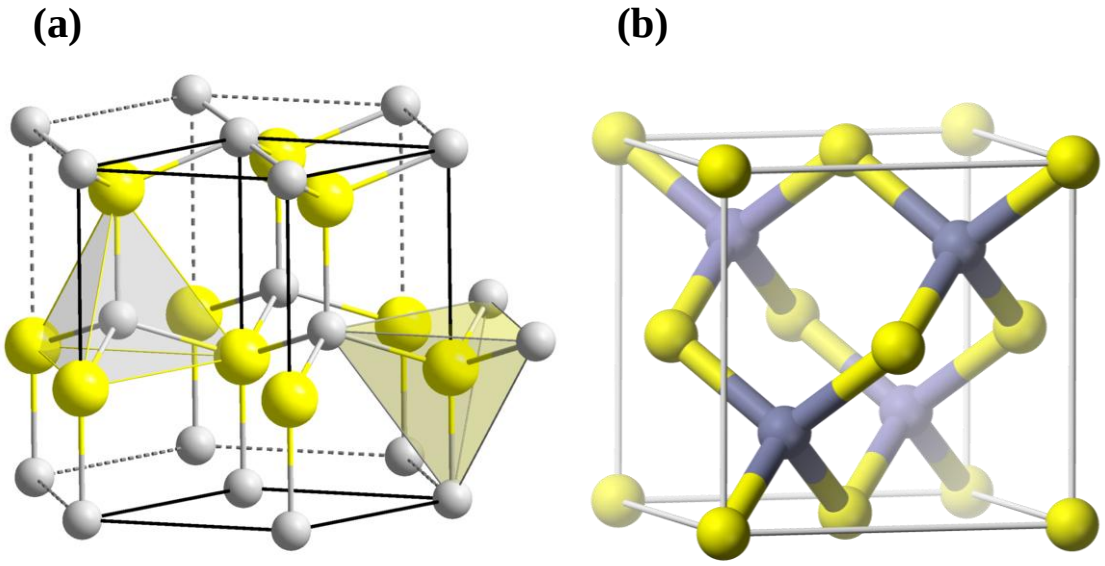

Figure 1.2 Crystal structures of ZnO polymorphs: **(a)** wurtzite, **(b)** zinc blende. [12]

Similar as TiO_2, the wide band-gap ZnO is stable and relatively harmless to the human body thus it can be used as pigments in paints (less opaque than TiO_2), or be used as an ingredient in sunscreen lotions. In the field of electronic ceramics, ZnO is famous for its application to circuit protection as varistors (**Figure 1.3**). The boundary (around 1 ~ 2 nm thick [14]) between each ZnO grain and its neighbor forms a diode junction. When a relatively small voltage is applied across the ZnO varistor, a tiny current flows which was caused by reverse leakage through the diode junctions. When a large voltage is applied, the diode junction breaks down due to a combination of thermionic emission [15] and electron tunneling, then a large current flows. The ZnO varistor has a high resistance at moderate low voltages and a low resistance at unexpected high voltages, and thus with this special character as a "sensible" shunt, circuits could be protected from sharply increased voltage.

ZnO has a direct band-gap of around 3.3 eV that makes ZnO have wide optoelectronic applications. Because the native doping of this material is oxygen vacancies, ZnO is a good n-type semiconductor even in the absence of doping of other elements. The electron mobility of ZnO is promising (the mobility of single crystal ZnO is > 200 $cm^2/V \cdot sec$ at room temperature [16]) that makes ZnO films a potential active layer material in the next generation TFT used in flexible and transparent electronic devices. However, because of the nature of this material, it is not easy to deposit a dense and flat thin film with nanoscale thickness by solution processes.

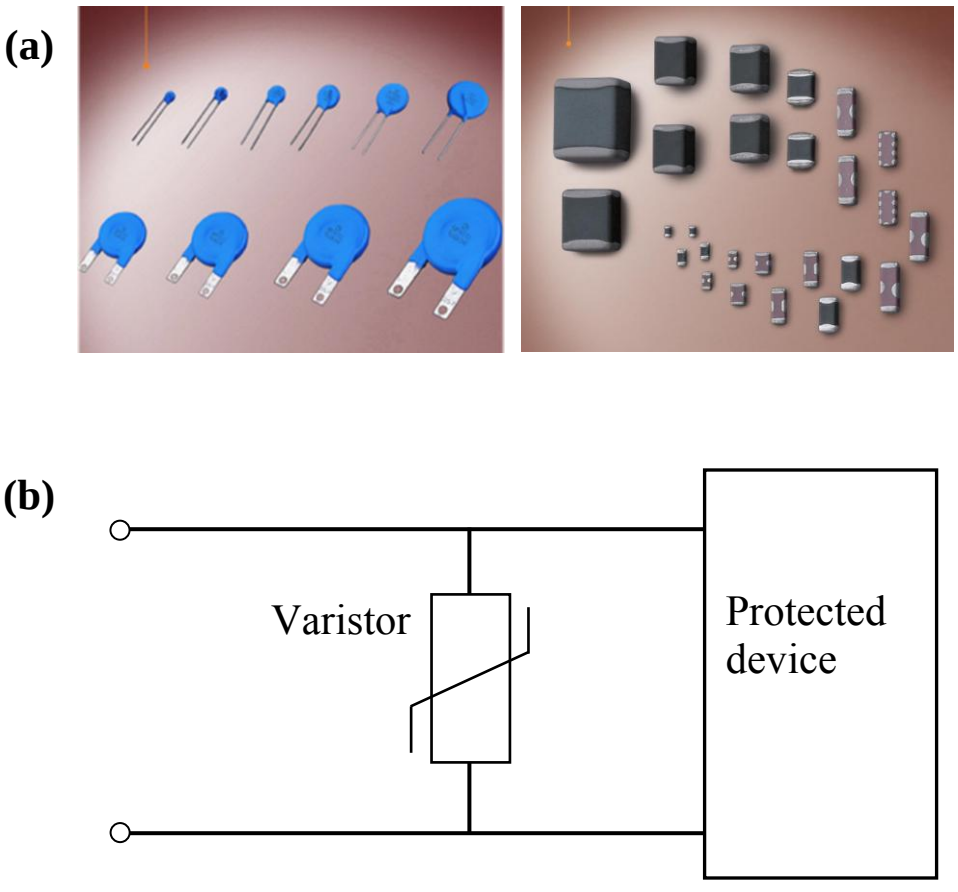

Figure 1.3 **(a)** Commercialized ZnO varistors, the right picture shows the ZnO chip varistors (AC Electro Co.), **(b)** schematic circuit of varistor protection.

1.3.3 Amorphous oxide semiconductors

Since 1990s, the revolution in display technology for lighter and thinner screens (e.g. liquid crystal displays - LCDs) made the research of transparent conducting thin films thrive. With successful development of transparent conducting oxides (TCO), wide band-gap amorphous oxides have attracted much interest because high transparency to visible light generally is not compatible with high electrical conductivity in normal metal conductors, such as aluminum or silver. Moreover, not only the display technology, the speedy developments of optoelectronic devices such as solar cells and OLEDs keep stimulating demands for transparent conductors.

The Hosono's group in Tokyo Institute of Technology has studied wide band-gap oxides for more than one decade and accumulated knowledge and experience of preparing transparent oxide films and fabricating devices made of these films [17~20]. In 2004, Nomura et al. proved the room-temperature fabrication of transparent flexible thin-film transistors using amorphous-IGZO (a-IGZO) semiconducting films, and initiated the studies of using amorphous oxide semiconductors (AOSs) to be the active layers of "transparent" TFT [21].

Figure 1.4a illustrates the charge carrier transport paths (the wave-function of the conduction band bottom) in AOSs. The bottom of the conduction band in this kind of oxides that have high ionicity is primarily composed of spatially spread metal *ns* orbitals with isotropic shape (*n* is the "large" principal quantum number, $n > 4$), and the overlap among adjacent metal *ns* orbitals is possible. Because the magnitude of this overlap is insensitive to the distorted chemical bonds exist in AOSs, the mobilities of typical AOSs could be similar to those of the corresponding crystalline forms (**Figure 1.4b**).

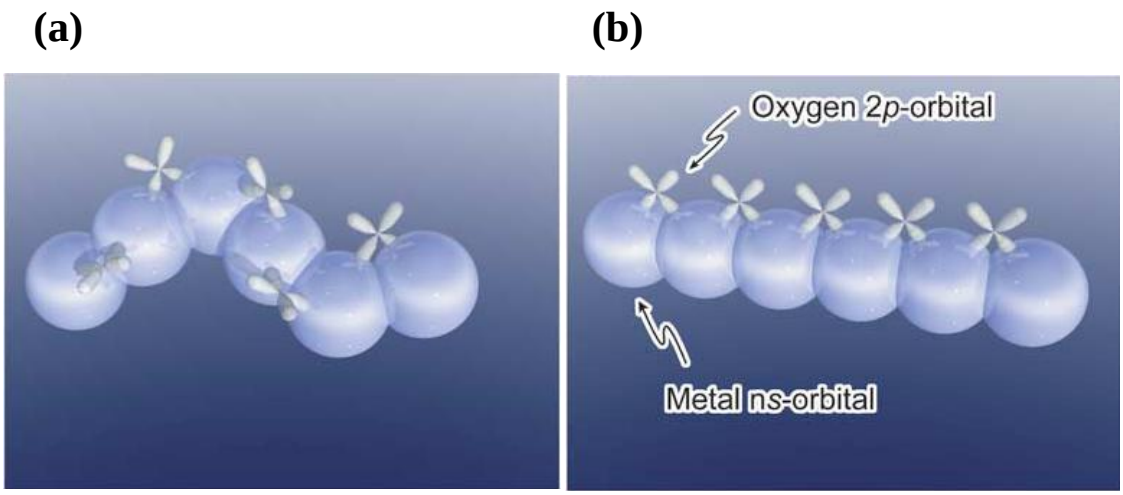

Figure 1.4 Schematic orbital drawings for the carrier transport paths in amorphous **(a)** and crystalline **(b)** oxide semiconductors. Spheres denote metal *s* orbitals. Direct overlap between adjacent metal *s* orbitals is rather large, and is not significantly affected even in an amorphous structure [21]. (The orbitals shown are illustrative, and do not show exact wave-functions)

The phenomenon described above could also explain why many transparent conductive oxides (e.g. ITO) are composed of heavy post transition metal cations such as In^{+3} and Sn^{+4}. Moreover, because of the fourfold coordination in ZnO crystal structure, the small Zn–Zn distance makes the formation of greatly dispersed conduction band bottom more easily and then results in high electron mobility. Furthermore, there is another important factor that needs to be considered: many oxide semiconductors have uncontrollable high carrier concentrations because oxygen vacancies are easily formed and generate excess free electrons. To suppress the generation of the free carriers via the formation of oxygen vacancies, the incorporation of stronger metal–oxygen bonds would be effective [22].

Based on the principles above proposed by Hosono et al., the intension of designing a-IGZO as the AOS active layer could be: the combination of In_2O_3 and

ZnO could give the oxide products possess high electron mobility, and the introducing of Ga could offer stronger chemical bonds between metal and oxygen that reduces the concentration of free carriers.

The majority of reports in the literature have demonstrated TFTs using high field-effect mobility ($\geq$ 10 $cm^2/V{\cdot}sec$) a-IGZO films as the active layer, which were generally deposited in vacuum environment (with pulsed laser deposition or rf sputtering process). The requirement of vacuum environment would slow the fabrication of electronic devices, increase the cost of processing, and also limit the large-scale manufacturing of related electronic products. In order to make the manufacture of large-scale and large-area transparent integrated circuits on flexible plastic substrates economically feasible, liquid phase processes for depositing AOSs thin films at atmospheric pressure have to be developed promptly.

1.4 Research purposes and objectives

In order to realize the fabrication of new generation low-cost electronics with novel characteristics and functionalities such as flexibility and transparency while also retaining desired device qualities (e.g. good stability, long life time), wide band-gap oxide films have been incorporated into organic electronic devices so as to take advantage of the merits of both classes of materials. To achieve the ambitious goal described above, the development of advanced solution-base processes for preparing oxide films under special conditions (e.g. low temperatures, atmospheric pressure) is absolutely critical.

In my doctoral study, I investigated every step in the fabrication process of

oxide/organic hybrid devices, from the synthesizing of nanoparticles and preparation of thin films to the fabrication and measurement of devices.

The objectives of my research are:

1. Synthesizing wide band-gap oxide nanoparticles with high dispersibility.
2. Preparing crystalline oxide thin films at low temperature and applying the oxide films to polymer electronic devices.
3. Improving the performance of oxide/organic hybrid devices by reforming the interface between oxide nanoparticles and semiconducting polymer.
4. Fabricating amorphous oxide semiconducting thin film transistors (TFT) with a special solution deposition process of amorphous oxide active layers.

The results of the above-mentioned research efforts as well as their further discussion are presented in this dissertation; the outline is listed as below:

In this first chapter, the motivation for working on combining wide band-gap oxide thin films with organic electronics was given. A background on wide band-gap oxides as well as the deposition technologies of oxide thin films was reviewed.

Chapter 2 demonstrates the feasibility of preparing crystalline TiO_2 thin films at room temperature and applying the as-prepared TiO_2 thin films to polymer/TiO_2 optoelectronic devices. This work had been published in *Organic Electronics* (2011, vol. 12, pp. 1073).

In chapter 3, characterizations of synthesized TiO_2 nanoparticles are presented. According to the characterization results of nanoparticles, the performance of

fabricated polymer/TiO_2 hybrid LEDs could be improved largely by post-annealing to further remove the hydroxyl groups attached on the particle surface and densify the oxide/polymer bilayer. Manuscripts of this work are in preparation.

Chapter 4 describes a solution process for the deposition of amorphous-IGZO thin films. The good performance of TFT devices using the prepared a-IGZO films as the active layers demonstrates the potential of this novel process. A manuscript of this work is currently being prepared for submission.

REFERENCES

[1] S.C. Tse, H.H. Fong, S.K. So, J. Appl. Phys. 94 (2003) 2033.

[2] H.H. Fong, S.K. So, J. Appl. Phys. 98 (2005) 023711.

[3] H. Aziz, Z. Popovic, C.P. Tripp, N.-X. Hu, A.-M. Hor, G. Xu, Appl. Phys. Lett. 72 (1998) 2642.

[4] T. Aoyama, S. Saida, Y. Okayama, M. Fujisaki, K. Imai, T. Arikado, J. Electrochem. Soc. 143 (1996) 977.

[5] T. Maruyama, T. Kanagawa, J. Electrochem. Soc. 143 (1996) 1675.

[6] D. A. H. Hanaor, C. C. Sorrell, J. Mater. Sci. 46 (2011) 855.

[7] Joseph Smyth, Mineral Structure Data, University of Colorado, http://ruby.colorado.edu, (accessed 3/29/2011).

[8] B. O'Regan, J. Moser, M. Anderson, M. Grätzel, J. Phys. Chem. 94 (1990) 8720.

[9] B. O'Regan, M. Grätzel, Nature 353 (1991) 737.

[10] K. Morii, M. Ishida, T. Takashima, T. Shimoda, Q. Wang, Md. K. Nazeeruddin, M. Grätzel, Appl. Phys. Lett. 89 (2006) 183510.

[11] H.J. Bolink, E. Coronado, D. Repetto, M. Sessolo, E.M. Barea, J. Bisquert, G. Garcia-Belmonte, J. Prochazka, L. Kavan, Adv. Funct. Mater. 18 (2008) 145.

[12] Zinc oxide, Wikipedia, http://en.wikipedia.org/wiki/Zinc_oxide, (accessed 4/3/2011).

[13] C. H. Bates, W. B. White, R. Roy, Science 137 (1962) 993.

[14] Y.-M. Chiang, H. Wang, J.-R. Lee, J. Microscopy 191 (1998) 275.

[15] A. Kusy, T. G. M. Kleinpenning, J. Appl. Phys. 54 (1983) 2900.

[16] W. Lin, D. Chen, J. Zhang, Z. Lin, J. Huang, W. Li, Y. Wang, F. Huang, Cryst. Growth Des. 9 (2009) 4378.

[17] H. Hosono, N. Kikuchi, N. Ueda, H. Kawazoe, J. Non-Cryst. Solids 198-200 (1996) 165.

[18] M. Orita, H. Ohta, M. Hirano, S. Narushima, H. Hosono, Philos. Mag. B 81 (2001) 501.

[19] S. Narushima, M. Orita, M. Hirano, H. Hosono, Phys. Rev. B 66 (2002) 35203.

[20] K. Nomura, H. Ohta, K. Ueda, T. Kamiya, M. Hirano, H. Hosono, Science 300 (2003) 1269.

[21] K. Nomura, H. Ohta, A. Takagi, T. Kamiya, M. Hirano, H. Hosono, Nature 432 (2004) 488.

[22] K. Nomura, A. Takagi, T. Kamiya, H. Ohta, M. Hirano, H. Hosono, Jpn. J. Appl. Phys. 45 (2006) 4303.

CHAPTER 2

ROOM-TEMPERATURE PREPARATION OF CRYSTALLINE TiO_2 THIN FILMS AND THEIR APPLICATION IN POLYMER/TiO_2 HYBRID OPTOELECTRONIC DEVICES

2.1 Abstract

Highly homogeneous crystalline TiO_2 thin films with very low surface roughness were prepared by spin-coating of a TiO_2 nanoparticle aqueous dispersion at room temperature without further heat treatment. Using these films as electron transporting layers, inverted structure hybrid photovoltaic cells (TiO_2/P3HT) and light-emitting diodes (TiO_2/F8BT) were demonstrated. The photovoltaic cells exhibited an energy conversion efficiency of 0.26 %, which is similar to that of cells utilizing TiO_2 layers sintered at high temperatures. Moreover, the light-emitting diodes showed an efficiency of 0.65 cd/A, which is higher than obtained from a reference inverted diode (0.1 cd/A). These measurements demonstrate that a properly designed nanoparticle casting route can help avoid high temperature crystallization or sintering steps for TiO_2 thin films, paving the road for their use in conjunction with plastic substrates.

2.2 Introduction

Organic electronic devices have attracted considerable interest from the electronic industry due to their facile processing; polymer coatings can be easily applied over large areas and to a variety of substrates, including mechanically flexible ones [1]. Associated with the ease of processing is the potential for low-cost fabrication. However, device stability is still a challenging problem that limits large-scale manufacturing of organic electronics. This limitation originates primarily from the

stability of materials used to inject electrons in or extract them from the organic layers. Low work function metals or their halides are generally used for this purpose, but these materials are very sensitive to ambient conditions. Thus, fabrication at inert conditions and careful encapsulation of the final device are required, which increases the complexity of fabrication (and presumably the product cost).

The interest for stable electron injection/extraction materials has led to the investigation of inorganic compounds and the fabrication of hybrid devices: Layers consisting of materials such as Cs_2CO_3 [2], TiO_x [3,4], and ZnO [5-8], have been used in conjunction with stable electrodes to inject electrons to or extract them from organic layers. Among the many available materials, nanocrystalline titanium dioxide (TiO_2) shows a remarkable capacity for electron transport [9] and has been extensively used in applications such as dye-sensitized solar cells (DSSC) to extract electrons from a dye molecule [10]. Morii et al. has recently demonstrated organic light emitting diodes using a compact TiO_2 film as an electron injecting bottom electrode [11]. The film was deposited by a spray pyrolysis process using a titanium precursor solution. The disadvantage of this process is that it requires the substrates to be heated at 400 - 450 ℃ during pyrolysis, and at even higher temperatures (~ 500 ℃) for sintering the nanoparticles [12,13]. Such high temperatures are not compatible with the use of plastic substrates and prohibit the full integration of inorganic materials with organic electronics. To this end, low temperature atomic layer deposition (ALD) has also been used to make TiO_2 films [14,15]. However, a room temperature solution process would be the ultimate solution from the point of view of large-scale, cost-effective manufacture of electronic devices.

In this study, we report the synthesis of TiO_2 nanoparticles via a sol-gel process,

and the deposition of transparent TiO_2 thin films by spin-coating from an aqueous dispersion at room temperature, without any further heat treatment. We show that these films are suitable for applications in polymer optoelectronic devices (photovoltaic cells and light emitting diodes). The developed process yields TiO_2 thin films that are suitable for large-area deposition on practically any substrate, and thus it makes low cost, large-scale manufacturing of organic electronics possible in the not-so-distant future.

2.3 Experimental

2.3.1 Nanoparticle synthesis

TiO_2 was synthesized by hydrolysis of $TiCl_4$ (Fluka, 99.0%) at 40 °C in an aqueous solution containing hydrochloric acid (HCl, Fishersci.) and 2-propanol (Mallinckrodt) [16]. 1 mol/L $TiCl_4$ aqueous solution was prepared by dissolving $TiCl_4$ in a mixture of deionized (DI) water (18.2 MΩ Barnstead EASYpure® RoDI) and HCl (volume ratio of 19:1, H_2O:36-38% HCl). Because the reaction was highly exothermic and produced high quantities of fumes, $TiCl_4$ was added dropwise into the ice cooled HCl solution with vigorous stirring, and the reaction had to be carried out inside a fume hood. The $TiCl_4$ solution (4 mL) was filtered (syringe filter; 0.2 µm, Nylon, Millipore) and then added into a 2-propanol solution (32 mL of 2-propanol mixed with 4 mL of DI water). The obtained reaction mixtures were incubated at 40 °C in a water bath (Fishersci) for 12 hours, which led to the formation of white TiO_2 particles. The particles were separated by centrifugation, washed with ethanol, and then dried at 40 °C overnight.

Particle size and morphology were investigated by transmission electron microscopy (TEM, FEI Tecnai G2 T12, field emission gun, 120 kV), and thin film

sections were examined by field emission scanning electron microscopy (FESEM, Hitachi S4500, 10 kV) after being sputter-coated with Au/Pd. The crystal phase of the particles was determined by powder X-ray diffraction (XRD) in θ-2θ scan mode from 15°-80° (Scintag Inc., Theta-Theta Diffractometer; Radiation: Cu Kα1; Scan rate: 0.012 Deg/min; Step: 0.02°). The surface morphology of the films was examined with an atomic force microscope (AFM, DI 3100 Dimension microscope) using tapping mode. UV/Vis absorption spectra were obtained using a Shimadzu UV-3101PC UV/Vis/Near-IR Spectrophotometer; thin films to be measured were spin-coated on quartz slides to obtain accurate UV/Vis absorption spectra.

2.3.2 Device fabrication

Devices were fabricated on pre-patterned indium tin oxide (ITO)-coated soda lime glass substrates (<20 ohm/sq, Kintec, Hong Kong). Before thin film deposition, these substrates were cleaned by sonication in non-ionic detergent and DI water, and then treated with a 10-minute UV-ozone (Jelight) exposure.

The photovoltaic cells had a structure of glass/ITO/TiO_2 (15 nm)/P3HT (40 nm)/Au (50 nm). Before the TiO_2 thin film deposition, the TiO_2 nanoparticles were dissolved in DI water (5 – 10 mg/mL) to form a clear dispersion. TiO_2 thin films were deposited on top of cleaned ITO glass substrates by spin-coating. Prior to the deposition of P3HT (poly-3-hexylthiophene), the as-deposited TiO_2 thin films were treated in UV-ozone for 10 minutes to remove the surface contamination and also to increase the wettability of the film. P3HT (American Dye Source) was dissolved in chlorobenzene to a concentration of 10 mg/mL before it was spin-coated at 1,500 rpm in air on top of the TiO_2 layer. After P3HT deposition, the films were annealed on a hot-plate at 230 ℃ in N_2 atmosphere for 15 seconds and then cooled down slowly (~

40 min) to improve the crystallinity of P3HT. Finally, 50 nm of Au was thermally evaporated at 0.05 nm/s under high vacuum (~10^{-6} Torr) to form the anode of the devices.

The light emitting diodes had an inverted structure of glass/ITO/TiO_2 (10 nm)/Al_2O_3 (5 nm)/F8BT copolymer (75 nm)/WO_3 (20 nm)/Au (40 nm). Similar to photovoltaic cell fabrication, TiO_2 dispersed in DI water was spin-coated onto cleaned ITO glass substrates in air to yield films with thickness of about 10 nm. A 10-minute UV-ozone treatment of these films was followed by the deposition of 5 nm of Al, which was then oxidized under UV- ozone for 15 minutes. Subsequently, the F8BT light-emitting copolymer, namely poly[(9,9-dioctylfluorenyl-2,7-diyl)-co-(1,4-benzo-{2,1',3}-thiadiazole)], with 10% benzothiadiazole was spin coated. The F8BT copolymer had a molecular weight of 15,000 and a polydispersity of 3.0. It was dissolved in p-xylene to yield a solution of 15 mg/mL and was spin-coated at 1,000 rpm in a N_2 environment. Finally a top contact of WO_3 (20 nm)/Au (40 nm) was thermally evaporated at 0.1 nm/s and 0.05 nm/s, respectively.

2.4 Results and Discussion

TiO_2 nanoparticles were prepared by hydrolysis of $TiCl_4$ at 40 ℃ in an isopropanol based sol-gel environment. TEM images show that nanoparticles, which did not aggregate, were obtained with an average particle size of 2 ± 0.4 nm (**Figure 2.1a**). **Figure 2.2** shows the XRD pattern of as-prepared TiO_2 nanoparticles. From the XRD analysis, it is evident that both anatase and rutile structures exist in the sample, with anatase as the major phase. The XRD pattern of the formed phases is consistent with the data recorded in JCPDS file no. 21-1272 (anatase) and 21-1276 (rutile). The broad width of the diffraction peaks is attributed to the small crystallite size of the

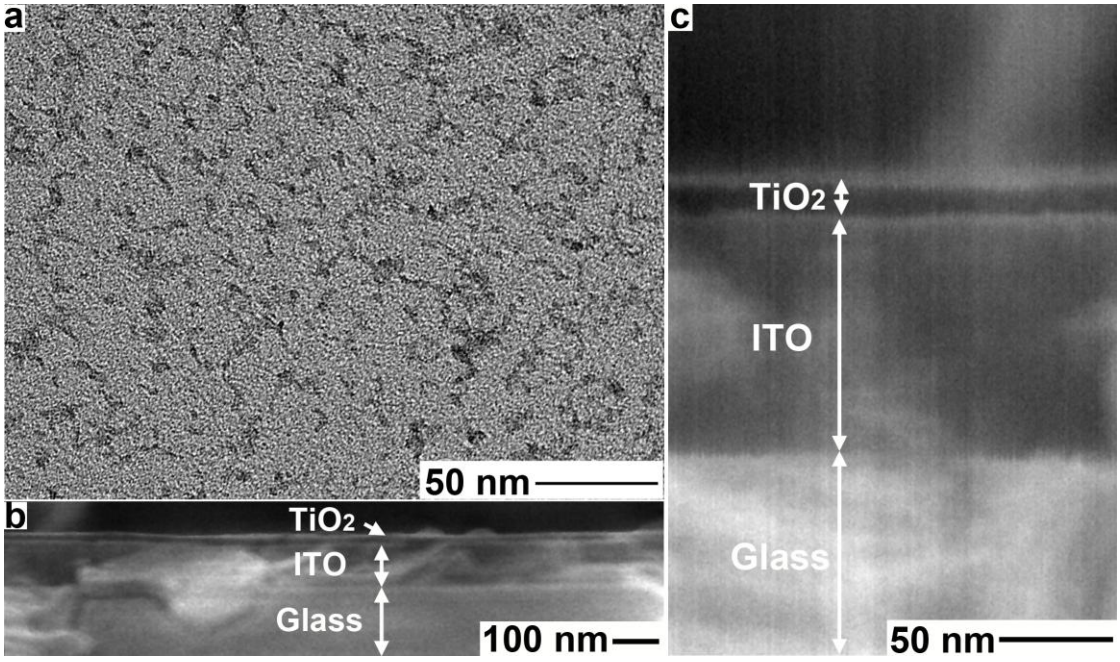

Figure 2.1 Micromorphology of prepared nano-sized TiO_2 materials, **a)** TEM image of the TiO_2 nanoparticles. **b, c)** FESEM image of a TiO_2 thin film deposited on ITO-coated glass substrate.

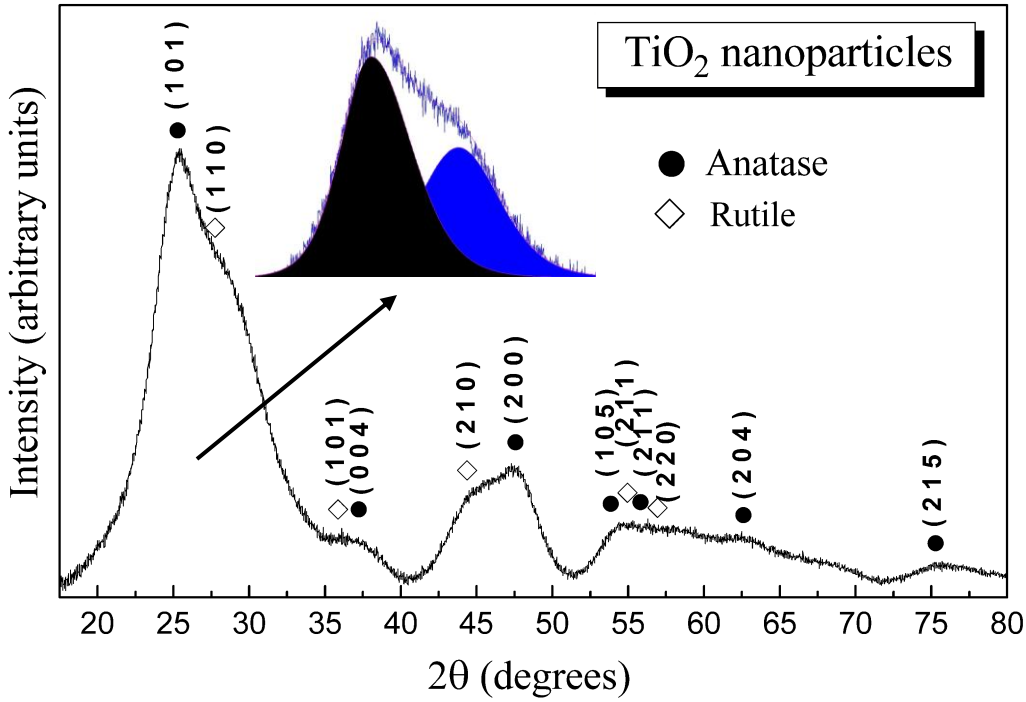

Figure 2.2 XRD pattern of the TiO_2 nanoparticles, the inset shows the deconvolution of two partially overlapping peaks – anatase (1 0 1) and rutile (1 1 0).

TiO_2 nanoparticles. The crystallite size of as-prepared TiO_2 nanoparticles could be calculated from the full width at half maximum of the (1 0 1) peak for anatase and (1 1 0) peak for rutile by the Debye–Scherrer formula (the distribution of these two partially overlapping peaks was analyzed with Pearson 7 waveform, as shown in the inset of **Figure 2.2**). It was found to be about 2 nm, which is consistent with the particle-size measured from TEM images.

One advantage of these nanoparticles is that they are easily dispersed in water and form a clear dispersion [17], which enables low-cost and environmental-friendly thin-film processing by means of spin-coating. No further annealing was needed to make our process more amenable to the fabrication of TiO_2/polymer hybrid devices, as compared to previously reported high-temperature processes [18-20]. A section of a typical TiO_2 thin film spin-coated on ITO coated soda-lime-glass substrate was examined by FESEM. The FESEM images show that the TiO_2 thin film is uniform in thickness along the section (**Figure 2.1b**) which was measured to be around 15 nm in the high-magnification image (**Figure 2.1c**). By adjusting the conditions of spin-coating, the thickness of TiO_2 films could be varied from several nanometers to the sub-micrometer scale.

The morphology of the as-prepared TiO_2 thin films on ITO glass substrate was investigated by AFM and it was found that it can be adjusted by changing the concentration of dispersion and the deposition conditions. Under specific conditions (high TiO_2 concentration and low spin speed, e.g. 10 mg/mL and 1000 rpm), rougher films with an RMS roughness (over a scan area of 10µm x 10µm) of 1.33 nm were obtained (**Figure 2.3a and 2.3b**). These TiO_2 films with a typical thickness around 15 nm were used for photovoltaics. In the case of TiO_2 thin films for use in LED

fabrication (typical thickness around 6 nm), the surface roughness could be significantly reduced by coating lower concentration dispersions with higher spin speeds (e.g. 5mg/mL, 9000 rpm). The RMS roughness of these smoother films (over a scan area of 10µm x 10µm) was only 0.6 nm (**Figure 2.3c and 2.3d**), similar to the surface roughness of the ITO coated glass substrate.

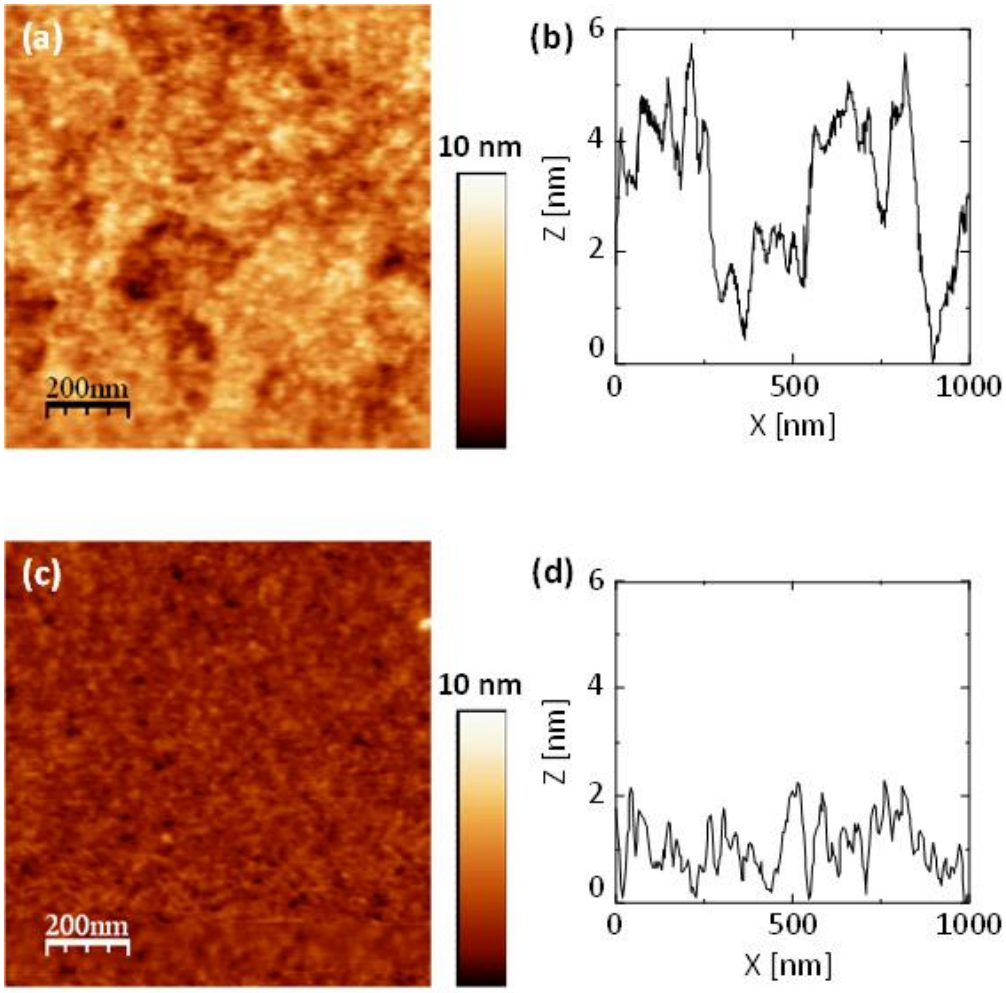

Figure 2.3 **a, b)** AFM images (left) and 1D profiles (right) for TiO_2 coated on ITO-coated glass for applications in photovoltaics. **c, d)** AFM images (left) and 1D profiles (right) for TiO_2 coated on ITO-coated glass for applications in polymer LEDs.

Photovoltaic cells were designed using room temperature deposited TiO_2 thin films as the electron extraction layer, while P3HT was spin-coated on top as the hole transporting layer. Annealing was applied after the deposition of P3HT on TiO_2 to improve the crystallinity of P3HT. In order to test the light absorption behaviour of TiO_2 and P3HT, UV/Vis absorption spectra of these films were measured (**Figure 2.4**). The UV/Vis absorption spectrum of the TiO_2 thin film exhibits an absorption onset at 350 nm, and the band-gap of about 3.5 eV was estimated from this absorption edge. The absorption onset is found to be blue-shifted as compared both to bulk rutile (~ 413 nm) and anatase (~ 387 nm) TiO_2, and this phenomenon could be attributed to the slightly twisted crystal structure since the size of nanocrystals comprising the TiO_2 thin films is only around 2 nm on average (**Figure 2.1a**) which makes the ordered range of nanocrystals not as long as the bulk TiO_2, and thus the nanosized crystals could tend to behave like amorphous titanium oxide with wider band gap [21,22]. TiO_2 absorbs in the UV range, while P3HT absorbs from about 350 nm to 650 nm, thus the TiO_2 layer has the potential to extend the spectral response of P3HT-based solar cells. Moreover, the TiO_2 layer can protect the polymer overlayer from photo-bleaching by absorbing UV light. **Figure 2.4** also shows the enhanced vibronic transitions in the UV/Vis spectrum of TiO_2/P3HT films. P3HT on TiO_2 thin film displays two discernible intrachain π–π^* absorption peaks at 560 and 610 nm, which is associated with stronger interchain interactions in more ordered polymers. This phenomenon was due to the slow cooling process after annealing, which increased the degree of order in P3HT on TiO_2. Similar behavior was also observed as P3HT deposited on ZnO layer with similar annealing/cooling treatment after [7].

The relationship between light absorption and photocurrent was examined by external quantum efficiency (EQE) measurements. Gold was chosen as top electrode

of the device due to its appropriate work function (~5.1 eV). EQE is a measure of the number of charge carriers collected in the external circuit for every photon that has been absorbed at a particular wavelength. It is calculated according to the formula:

$$EQE(\%) = \frac{100 \times 1240 \times J_{SC}}{\lambda \times P_{INC}} \qquad \text{(Equation 2.1)}$$

Figure 2.5 shows the EQE values for the hybrid photovoltaic device. The glass/ITO/TiO_2 (15 nm)/P3HT (40 nm)/Au (50 nm) device achieved an EQE of 5 % in the 500-550 nm spectral region. A shoulder in the 300-350 nm spectral region shows that the device also generates current in the UV region, which could be attributed to the contribution of the TiO_2 layer.

The open circuit voltage (V_{oc}), short circuit current (J_{sc}), fill factor (FF) and power conversion efficiency (PCE) of the hybrid photovoltaic cell under AM 1.5 100 mW/cm^2 illumination were calculated from the I-V curves. If P_{INC} is the power intensity of the incident solar radiation, then the solar cell PCE is defined as follows:

$$PCE = \frac{P_{MAX}}{P_{INC}} = \frac{V_{MAX} \times J_{MAX}}{P_{INC}} = \frac{FF \times V_{OC} \times J_{SC}}{P_{INC}} \qquad \text{(Equation 2.2)}$$

As shown in **Figure 2.6**, the hybrid photovoltaic cell achieved a V_{oc} of 0.50 V, a J_{sc} of 0.90 mA/cm^2, a FF of 0.58 and a PCE of 0.26 %. The efficiency of our photovoltaic cell is comparable to the efficiency (0.28% PCE) reported by Shen et al. of a photovoltaic cell with similar combination of materials (ITO/TiO_2/P3HT/Au) [23]. However, in that report, the TiO_2 thin films were deposited from a sol-gel precursor and required post annealing at 450° C, which is significantly higher than the process temperature reported here. In comparison to inverted devices based on ZnO layer, the

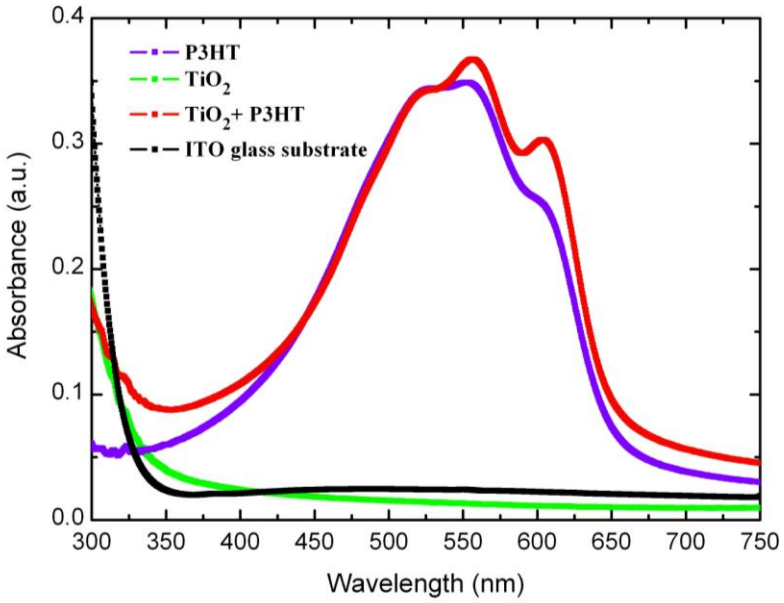

Figure 2.4 UV/Vis absorption for thin films of TiO_2, P3HT, a bilayer of the two (all on quartz), and the glass substrate used for device fabrication.

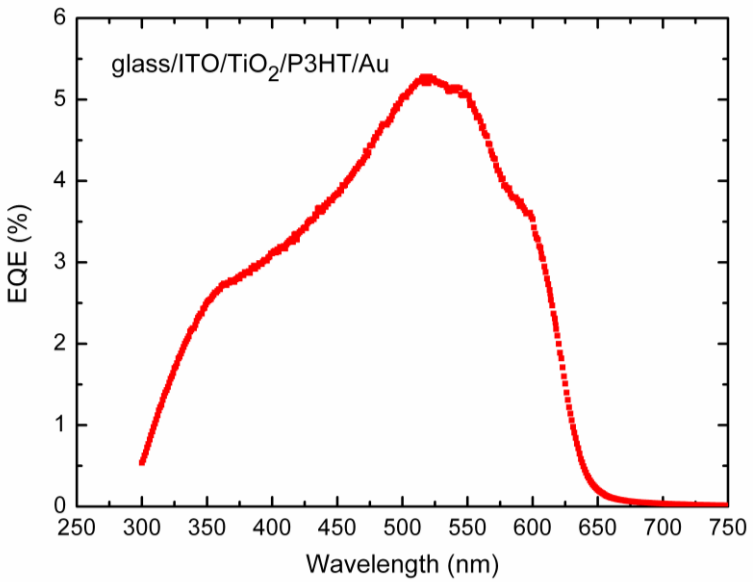

Figure 2.5 External quantum efficiency scan from an ITO/TiO_2/P3HT/Au device.

performance of TiO_2/P3HT photovoltaic cell reported here is better than the performance of bi-layer ZnO/P3HT devices [5], and is comparable to the ZnO

nanorod/P3HT composite devices (0.20 ~ 0.28 % PCE) [5,7]. However, the performance of ZnO/P3HT photovoltaic devices reported by Olson et al. shows an improved efficiency (0.53 % PCE) due to a mesoporous structure of ZnO nanofibers that were grown via a hydrothermal process [6].

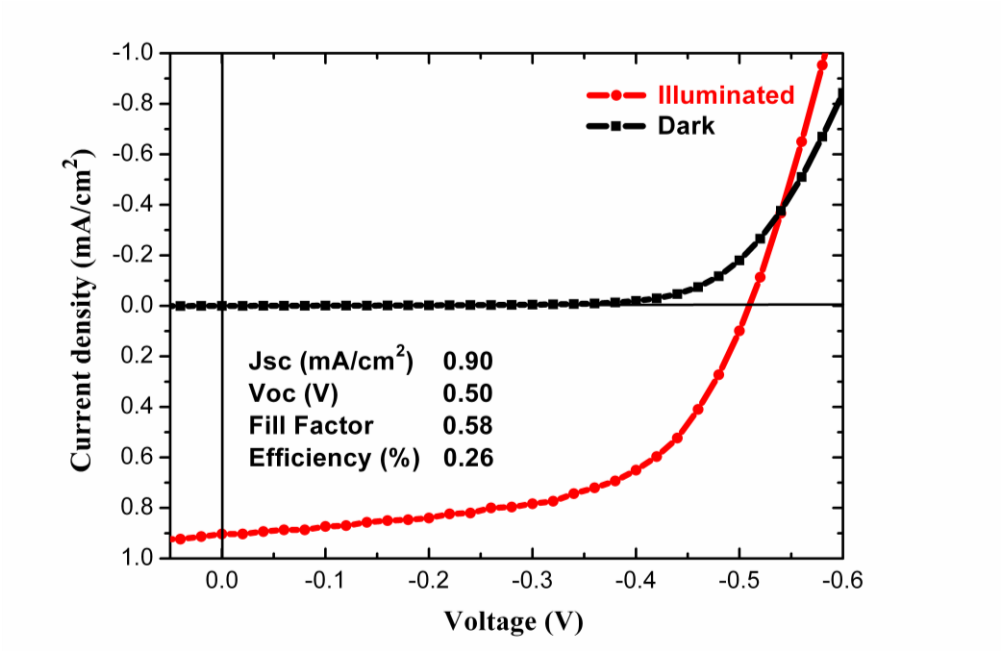

Figure 2.6 I-V curves of the photovoltaic cell.

We found that if we spin-coat TiO_2 thin films with suspensions dispersing larger size TiO_2 nanoparticles (e.g. P25 with the average particle size of about 21 nm, a generous gift from Degussa Corporation), the photovoltaic devices fabricated with the similar process as this study often suffer from large current leakage and poor photovoltaic response. This result is due to the rough surface of as-deposited TiO_2 layer with large nanoparticle clusters (~ 100 nm) "sprinkled" on the surface**.** A strong point of the process described in this letter is that smooth and homogeneous TiO_2 thin films with very small roughness can be prepared readily at room-temperature via a

liquid phase process. The good dispersibility and the good film forming properties can be attributed to the small and uniform size of the TiO_2 nanoparticles.

Figure 2.7a and **2.7b** show the current vs. voltage and luminance vs. voltage characteristics of the TiO_2/polymer hybrid light emitting diode with a structure of ITO/TiO_2 (10 nm)/Al_2O_3 (5 nm)/F8BT copolymer (75 nm)/WO_3 (20 nm)/Au (40 nm). The electroluminescence spectrum shows an emission peak at 536 nm (**Figure 2.7c**). This hybrid LED turns on at ~ 7 V and reaches 100 cd/m^2 at ~ 8.5V. The maximum brightness approaches ~ 4000 cd/m^2 at 12 V. The corresponding luminous efficiency at 100 mA/cm^2 is ~ 0.6 cd/A (**Figure 2.7d**). This value is 6 times higher than that of a reference inverted device (~ 0.1 cd/A) utilizing only ITO as the cathode (**Figures 2.7a, b, d,** circle symbols), and comparable to that of a reference typical bottom anode device (ITO/PEDOT:PSS (AI4083) (60 nm)/F8BT copolymer (75 nm)/CsF (1 nm)/Al (40 nm)), in which the turn-on voltage was ~ 4.5V, and the maximum brightness was ~ 4500 cd/m^2 at 9V.

Previous reports attempted to incorporate either dense or porous TiO_2 into inverted polymer LEDs by following different schemes. For example, by means of spray-pyrolysis using a titanium organic precursor on heated substrates and then annealing at 520 °C, to obtain dense TiO_2 films [13]. The corresponding hybrid light emitting diodes showed an efficiency of about 0.6 cd/A. In a second example, spin-coating of a TiO_2 colloidal suspension of nanoparticles, followed with sintering at 450 °C, yielded a mesoporous film structure [24]. This method was used to prepare a TiO_2 layer for hybrid light emitting diodes, which showed a substantially lower current efficiency [24,25] than the one we report here. Therefore, the devices reported here show comparable or better performance than light emitting diodes employing TiO_2 films

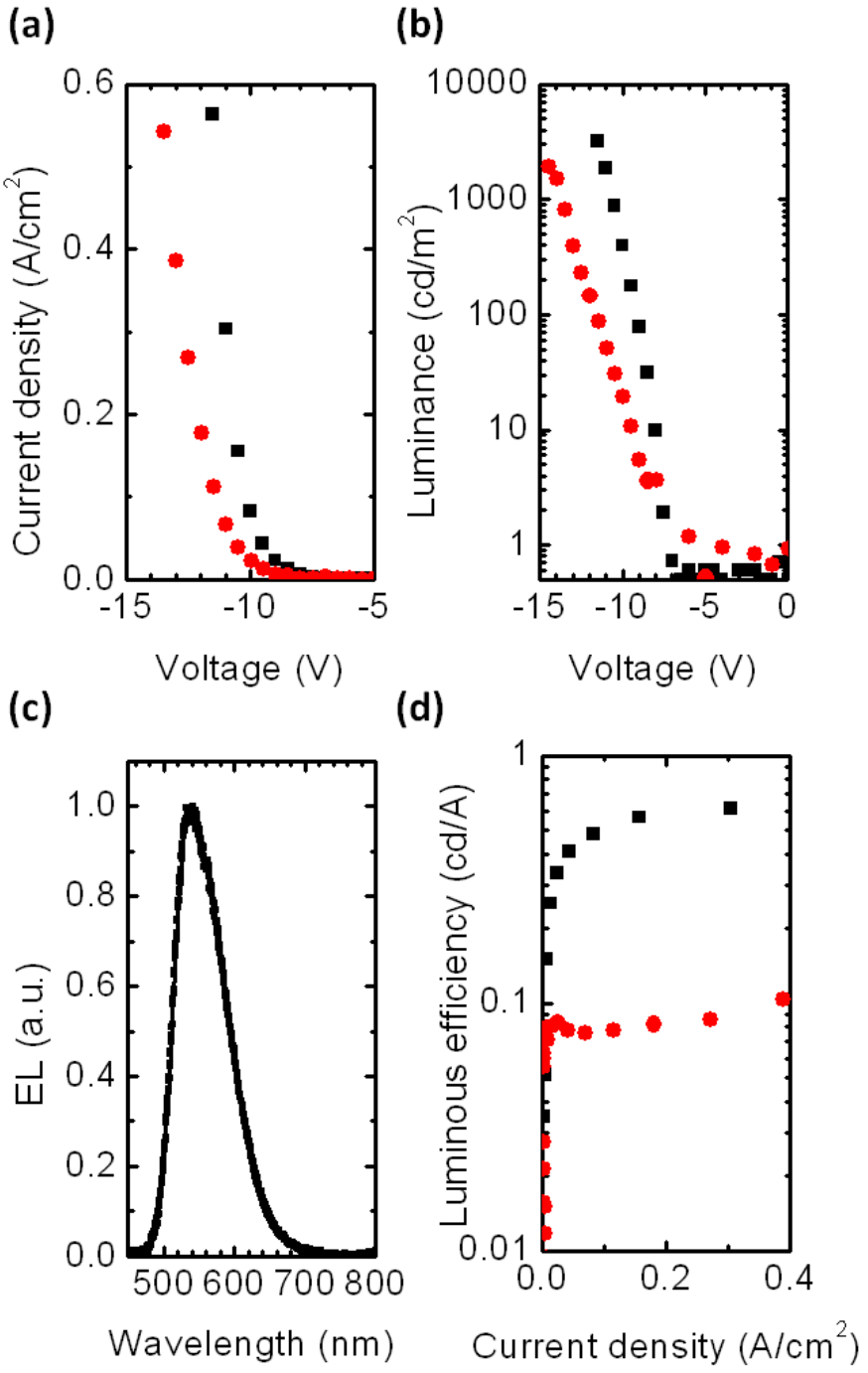

Figure 2.7 **a)** Current vs. voltage (J-V), **b)** Luminance vs. voltage (L-V) characteristics, **c)** EL spectrum, and **d)** luminous efficiency of a TiO_2/polymer hybrid LED. Data from two devices are shown: ITO/TiO_2/Al_2O_3/F8BT copolymer/WO_3/Au (squares ■) and one with a similar structure but utilizing only ITO as the cathode (circles ●).

prepared and sintered at higher temperatures. To the best of our knowledge, the data described here constitute the first demonstration of a room-temperature processed TiO_2 film for hybrid light emitting diodes.

2.5 Conclusion

In summary, we show that TiO_2 thin films suitable for polymer optoelectronic device fabrication can be prepared at room temperature via a properly designed liquid phase deposition process. TiO_2/P3HT photovoltaic cells show comparable performance to devices utilizing TiO_2 layers sintered at high temperatures. TiO_2/F8BT hybrid light emitting diodes show an efficiency of 0.65 cd/A. These results show that it is now possible to apply TiO_2 films to the fabrication of low cost organic devices.

REFERENCES

[1] G. Malliaras, R. Friend, Phys. Today 58 (2005) 53.

[2] H. H. Liao, L. M. Chen, Z. Xu, G. Li, Y. Yang, Appl. Phys. Lett. 92 (2008) 173303.

[3] K. Lee, J. Y. Kim, S. H. Park, S. H. Kim, S. Cho, A. J. Heeger, Adv. Mater. 19 (2007) 2445.

[4] T. Kuwabara, H. Sugiyama, M. Kuzuba, T. Yamaguchi, K. Takahashi, Org. Electron. 11 (2010) 1136.

[5] A. M. Peiro, P. Ravirajan, K. Govender, D. S. Boyle, P. O'Brien, D. D. C. Bradley, J. Nelson, J. R. Durrant, J. Mater. Chem. 16 (2006) 2088.

[6] D. C. Olson, J. Piris, R. T. Collins, S. E. Shaheen, D. S. Ginley, Thin Solid Films 496 (2006) 26.

[7] D. C. Olson, Y.-J. Lee, M. S. White, N. Kopidakis, S. E. Shaheen, D. S. Ginley, J. A. Voigt, J. W. P. Hsu, J. Phys. Chem. C 111 (2007) 16640.

[8] S. K. Hau, H. L. Yip, N. S. Baek, J. Zou, K. O'Malley, A. K.-Y. Jen, Appl. Phys. Lett. 92 (2008) 253301.

[9] B. O'Regan, J. Moser, M. Anderson, M. Grätzel, J. Phys. Chem. 94 (1990) 8720.

[10] B. O'Regan, M. Grätzel, Nature 353 (1991) 737.

[11] K. Morii, M. Ishida, T. Takashima, T. Shimoda, Q. Wang, Md. K. Nazeeruddin, M. Grätzel, Appl. Phys. Lett. 89 (2006) 183510.

[12] L. Kavan, M. Grätzel, Electrochim. Acta. 40 (1995) 643.

[13] H. J. Bolink, E. Coronado, D. Repetto, M. Sessolo, E. M. Barea, J. Bisquert, G. Garcia-Belmonte, J. Prochazka, L. Kavan, Adv. Funct. Mater. 18 (2008) 145.

[14] H. Kim, S. Sohn, D. Jung, W. J. Maeng, H. Kim, T. S. Kim, J. Hahn, S. Lee, Y. Yi, M.-H. Cho, Org. Electron. 9 (2008) 1140.

[15] B. W. Kang, W. S. Kim, C. M. Hwang, D. Y. Moon, J. J. Kim, J. G. Park, J. W. Park, Jpn. J. Appl. Phys. 49 (2010) 08JG05.

[16] W. Wang, B. H. Gu, L. Y. Liang, W. A. Hamilton, D. J. Wesolowski, J. Phys. Chem. B 108 (2004) 14789.

[17] P. Wang, D. J. Wang, H. Y. Li, T. F. Xie, H. Z. Wang, Z. L. Do, J. Colloid Interface Sci. 314 (2007) 337.

[18] L. B. Roberson, M. A. Poggi, J. Kowalik, G. P. Smestad, L. A. Bottomley, L. M. Tolbert, Coord. Chem. Rev. 248 (2004) 1491.

[19] K. Takahashi, Y. Takano, T. Yamaguchi, J. Nakamura, C. Yokoe, K. Murata, Synth. Met. 155 (2005) 51.

[20] A. Sergawie, T. Yohannes, T. Solomon, Synth. Met. 157 (2007) 75.

[21] Z. Zhang, P. A. Maggard, J. Photochem. Photobiol. A 186 (2007) 8.

[22] R.S. Davidson, C.L. Morrison, J. Abraham, J. Photochem. 24 (1984) 27.

[23] L. Shen, G. Zhu, W. Guo, C. Tao, X. Zhang, C. Liu, W. Chen, S. Ruan, Z. Zhong, Appl. Phys. Lett. 92 (2008) 073307.

[24] S. A. Haque, S. Koops, N. Tokmoldin, J. R. Durrant, J. Huang, D. D. C. Bradley, E. Palomares, Adv. Mater. 19 (2007) 683.

[25] D. Kabra, M. H. Song, B. Wenger, R. H. Friend, H. J. Snaith, Adv. Mater. 20 (2008) 3447.

CHAPTER 3

CHARACTERIZATION OF REDISPERSIBLE TiO_2 NANOPARTICLES AND IMPROVING PERFORMANCE OF PLOYMER/TiO_2 HYBRID LIGHT EMITTING DIODES BY POST-ANNEALING

3.1 Introduction

Considerable research has been focused on nanosized oxide particles because of their novel size-dependent properties and wide range of important applications. For example, nanocrystalline TiO_2 was of great interests owing to its potential applications in many aspects such as photocatalysis, optical data storage, dye-sensitized solar cells and electron injection layer in organic light-emitting diodes (OLED) etc. [1]. In the past decades, nanoparticles synthesized by artfully designed processes with various conditions have been extensively studied. Besides the synthesis, the dispersibility of nanoparticles is also a very crucial issue in practical applications. As the size of particles getting smaller, the surface area as well as the surface energy of these tiny solids become larger that makes the nanoparticles agglomerate easily and then weakens their benefits of being nanosized. Thus, to prepare stable dispersion of nanoparticles without agglomeration is just the fundamental requirement for the technological applications of nanoparticles.

In this study, we describe a simple process to synthesize water-redispersible TiO_2 nanoparticles. The prepared TiO_2 nanoparticles were characterized by XRD, TEM, TGA, DLS and FT-IR. The TiO_2 nanoparticle dispersions were used to deposit TiO_2 thin films that are suitable for the application of organic electronics fabrication. With

the understanding of surface conditions of water-redispersible TiO_2 nanoparticles, the performance of TiO_2/polymer hybrid light-emitting diodes (LEDs) applying the deposited TiO_2 nanoparticles could be further improved by post-annealing treatment that removed the hydroxyl groups attached on the surface of nanoparticles and then formed a good bulk heterjunction between TiO_2 and light emitting polymer.

3.2 Experimental

3.2.1 Nanoparticle synthesis and characterization

TiO_2 was synthesized by hydrolysis of $TiCl_4$ (Fluka, 99.0%) at 40 ℃ (typical condition) in an aqueous solution containing hydrochloric acid (HCl, Fishersci.) and 2-propanol (IPA, Mallinckrodt) [2]. 1 mol/L $TiCl_4$ aqueous solution was prepared by dissolving $TiCl_4$ in a mixture of deionized (DI) water (18.2 MΩ Barnstead EASYpure® RoDI) and HCl (volume ratio of 19:1, H_2O:36-38% HCl). Because the reaction was highly exothermic and produced high quantities of fumes, $TiCl_4$ was added dropwise into the ice cooled HCl solution with vigorous stirring, and the reaction had to be carried out inside a fume hood. The $TiCl_4$ solution (4 mL) was filtered (syringe filter; 0.2 μm, Nylon, Millipore) and then added into a 2-propanol solution (total volume 36 mL, mixing 2-propanol and DI water with varied volume combinations). The obtained reaction mixtures were incubated at 40 ℃ in a water bath (Fishersci) for 12 hours, which led to the formation of white TiO_2 particles. The particles were separated by centrifugation and dried at a temperature lower than 40 ℃ overnight (due to the temperature control system of oven, the drying temperatures varied in a range from 35 – 40 ℃). For nanoparticles used to deposit thin films for device usage, rinsing slightly with ethanol was performed before overnight drying. The preparation procedure is schematized as the flow diagram (**Figure 3.1**)

Particle size and morphology were investigated by transmission electron microscopy (TEM, FEI Tecnai G2 T12, field emission gun, 120 kV), and thin film sections were examined by field emission scanning electron microscopy (FESEM, Hitachi S4500, 10 kV) after being sputter-coated with Au/Pd. The zeta potentials and Dynamic Light Scattering (DLS) particle sizing of TiO_2 nanoparticles were also measured (Malvern Inc. Zetasizer Nano). The crystal phase of the particles was determined by powder X-ray diffraction (XRD) in θ-2θ scan mode (Scintag Inc., Theta-Theta Diffractometer; Radiation: Cu Kα1; Scan rate: 0.012 Deg/min; Step: 0.02°). Fourier Transform Infrared Spectrometer (FT-IR) spectra of as-synthesized nanoparticles were recorded by Attenuated Total Reflectance (ATR) FT-IR spectroscopy. The chemical states of titanium and oxygen presented in the deposited thin films were analyzed by X-ray photoelectron spectroscopy (XPS, Surface Science Instruments SSX-100, monochromatic Al Kα; 1486.6 eV) at a take-off angle of 90°.

3.2.2 Device fabrication

Devices were fabricated on pre-patterned indium tin oxide (ITO)-coated soda lime glass substrates (<20 ohm/sq, Kintec, Hong Kong). Before thin film deposition, these substrates were cleaned by sonication in non-ionic detergent and DI water, and then treated with a 10-minute UV-ozone (Jelight) exposure.

The light emitting diodes had an inverted structure of glass/ITO/TiO_2 (40 nm)/Al_2O_3 (5 nm)/F8BT copolymer (120 nm)/WO_3 (20 nm)/Au (40 nm). Before the TiO_2 thin film deposition, the TiO_2 nanoparticles were dissolved in DI water (50 mg/mL) to form dispersion. TiO_2 thin films were spin-coated three times onto cleaned ITO glass substrates in air to yield films with thickness of about 50 nm. A 10-minute UV-ozone treatment of these films was followed by the deposition of 5 nm of Al,

which was then oxidized under UV- ozone for 15 minutes. Subsequently, the F8BT light-emitting copolymer, namely poly[(9,9-dioctylfluorenyl-2,7-diyl)-co-(1,4-benzo-{2,1',3}-thiadiazole)], with 10% benzothiadiazole was spin coated. The F8BT copolymer obtained from American Dye Source (ADS) Inc. had a molecular weight of 15,000 and a polydispersity of 3.0. It was dissolved in p-xylene to yield a solution of 15 mg/mL and was spin-coated at 1,000 rpm in a N_2 environment. After the deposition of polymer layer, the substrates with TiO_2/polymer bilayer on top were annealed at 300 ℃ under N_2 for 2 hours. Secondary ion mass spectroscopy (SIMS) was conducted to determine the depth profiles of TiO_2/F8BT bilayer before and after annealing. A top contact of WO_3 (20 nm)/Au (40 nm) was thermally evaporated at 0.1 nm/s and 0.05 nm/s, respectively under high vacuum (~10^{-6} Torr) to form the anode of the devices. The structure of our hybrid TiO_2/polymer LED is illustrated in **Figure 3.2**.

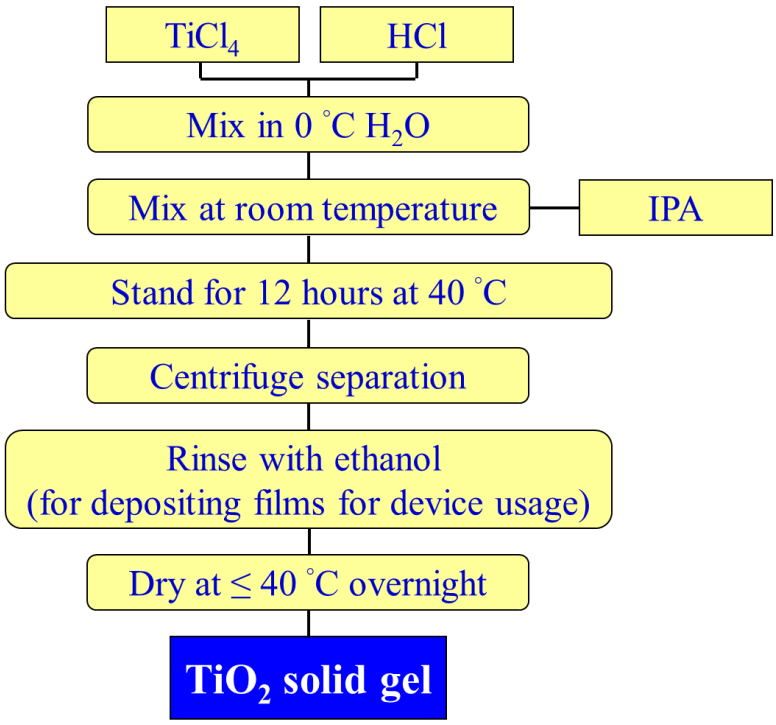

Figure 3.1 Flow diagram presenting the synthesis procedure of TiO_2 nanoparticles .

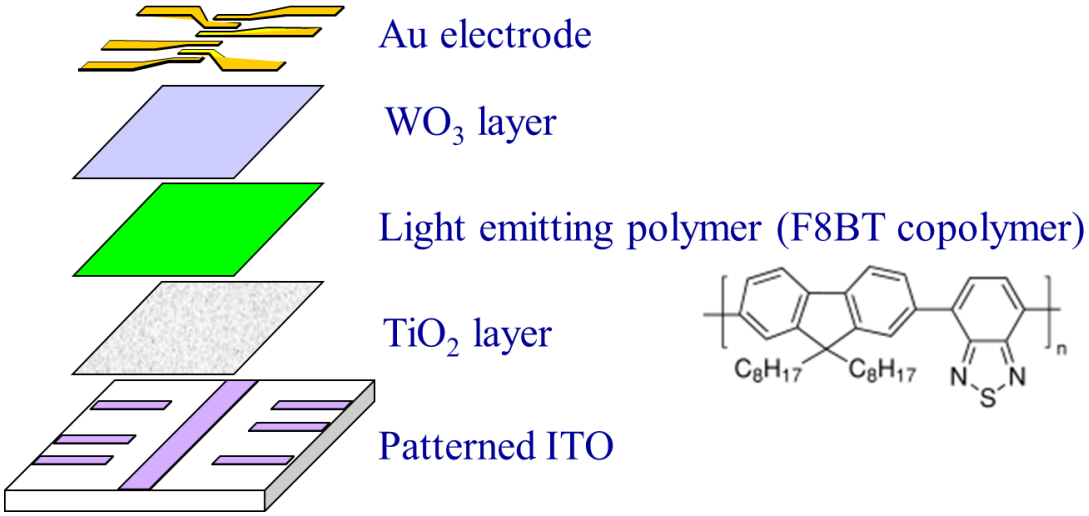

Figure 3.2 Hybrid TiO_2/polymer LED structure.

3.3 Results and Discussion

3.3.1 Characterization of synthesized TiO_2 nanoparticles

The TiO_2 nanoparticles were synthesized at 40 ℃ with different H_2O/IPA ratios while keeping the concentration of $TiCl_4$ in reactant solutions fixed at 0.1 mol/L. **Figure 3.3** shows the selected XRD patterns of synthesized nanoparticles. The ratio of anatase to rutile could be varied by changing the condition of H_2O/IPA ratios, however, as the ratio of H_2O/IPA larger than 1, the yield of the TiO_2 was decreased remarkably and the little amount of obtained TiO_2 was characterized pure rutile structure with the crystal size around 5 nm. Larger anatase/rutile ratio (75 % anatase to 25 % rutile) could be reached when the H_2O/IPA ratio ranged between 7/29 and 10/26 (the total volume of H_2O and IPA mixture was fixed at 36 ml), yet the particle sizes of TiO_2 nanoparticles obtained in this range were observed sharply increased comparing to the typical TiO_2 nanoparticles used in device fabrication (anatase/rutile ~ 2, $TiCl_{4\,(aq)}$: H_2O : IPA = 4 ml : 4 ml : 32 ml, labeled 4-4-32). **Figure 3.4** shows the

TEM micrographs of two anatase-rich TiO_2 nanoparticles. The typical TiO_2 nanoparticles (4-4-32) used in our hybrid devices were sized around only 2 nm, but the particle size of sample with more anatase phase content (anatase/rutile ~ 3, $TiCl_{4\,(aq)}$: H_2O : IPA = 4 ml : 9 ml : 27 ml, labeled 4-9-27) was around 40 ~100 nm, which was one order larger than the 4-4-32 sample. The results of particle sizes measured by DLS agree with the observation of micrograph in substance (**Figure 3.5**), though the particle size of 4-4-32 sample measured by DLS was around 6 nm, which is doubtful due to the size of these particles was smaller than the lower detection limit of DLS (normally 5 nm, depending on particle).

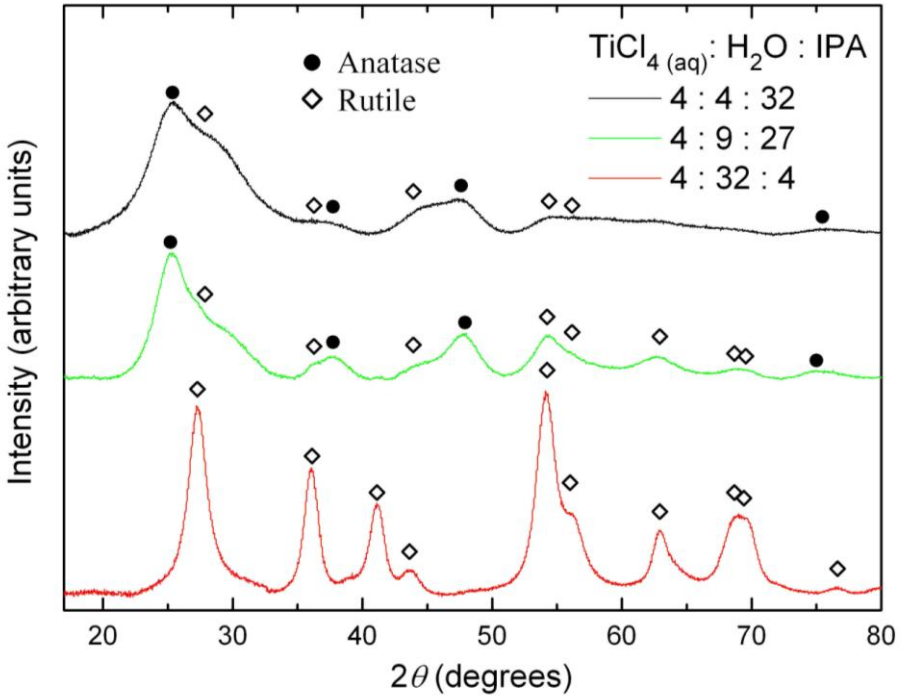

Figure 3.3 XRD patterns of the TiO_2 nanoparticles synthesized with different H_2O/IPA ratios.

The nanoparticles used in device fabrication (sample 4-4-32) dispersed well in water. **Figure 3.6a** shows the photograph of nanoparticle dispersions comparing TiO_2 synthesized in this study (4-4-32) and the commercialized P25 TiO_2. Clear dispersions

of sample 4-4-32 were obtained even the concentration of nanoparticles was increased to 50 mg/ml and the dispersions could be stable for more than 10 days without precipitation. The dispersion of synthesized TiO_2 nanoparticles with larger particle size (sample 4-9-27) was not that clear (**Figure 3.6b**), and the stability of this more turbid dispersion was not as good either that precipitation was observed after 3~4 days. The better stability of sample 4-4-32 dispersion was attributed to the much smaller particle size than sample 4-9-27, while the zeta-potentials of these two samples were measured with small difference (**Figure 3.7**). With the observations above, considering the particle size and the stability of nanoparticle aqueous dispersion, the TiO_2 nanoparticles applied to TiO_2/polymer hybrid LED fabrication were kept using the 4-4-32 sample through the study.

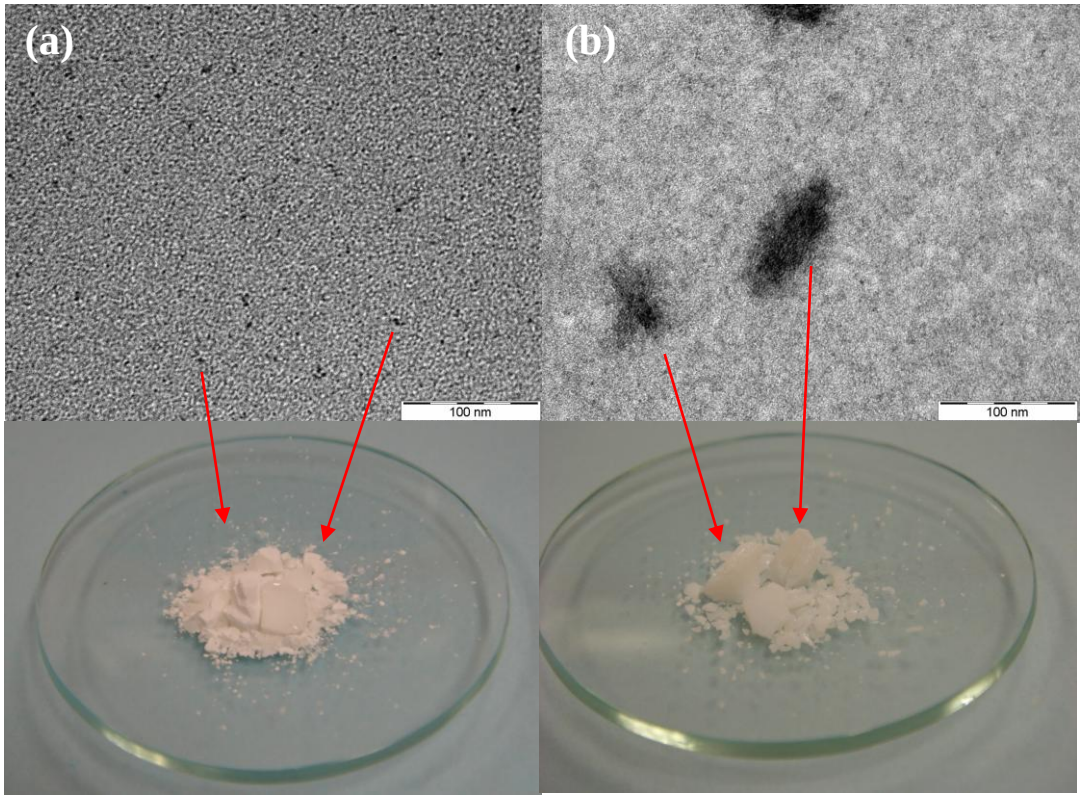

Figure 3.4 TEM images of prepared nano-sized TiO_2 nanoparticles, **(a)** $TiCl_{4\,(aq)}$: H_2O : IPA = 4 ml : 4 ml : 32 ml, labeled 4-4-32; **(b)** $TiCl_{4\,(aq)}$: H_2O : IPA = 4 ml : 9 ml : 27 ml, labeled 4-9-27.

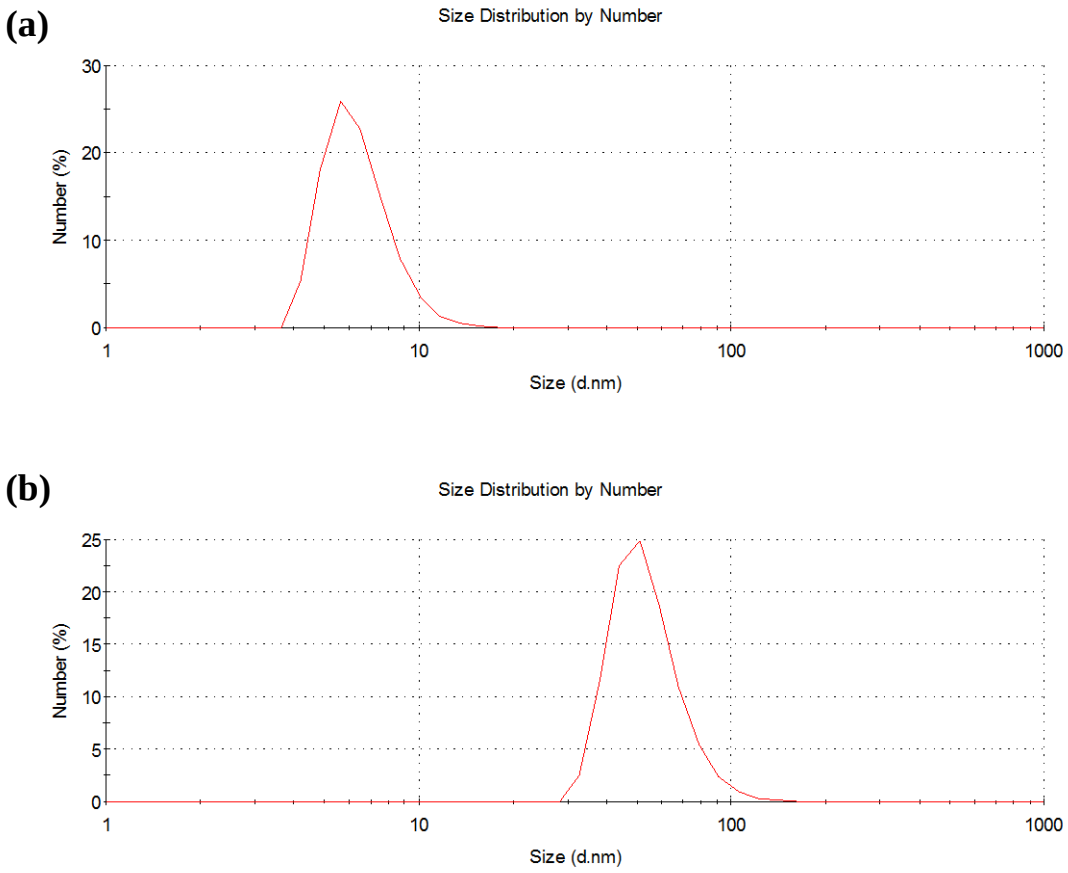

Figure 3.5 DLS results of **(a)** sample 4-4-32; **(b)** sample 4-9-27.

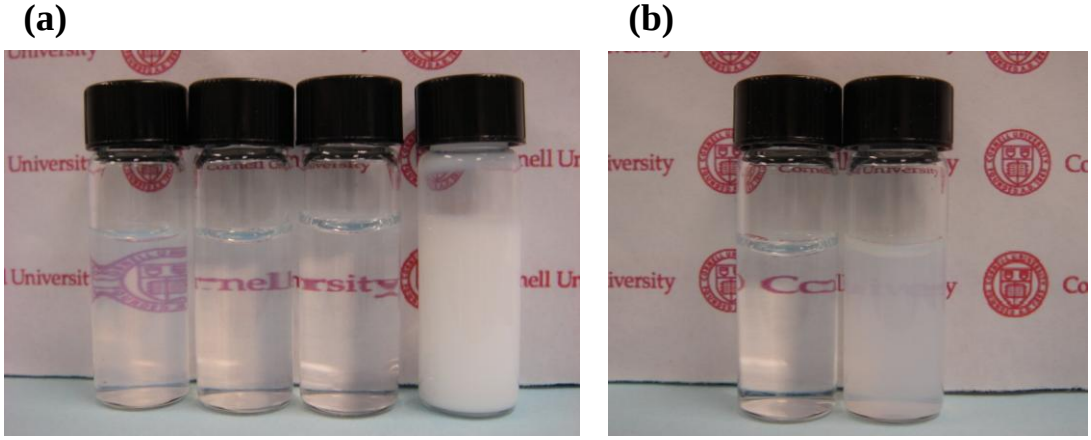

Figure 3.6 Photographs of nanoparticle dispersions, **(a)** sample 4-4-32, from left to right: 50 mg/ml, 30 mg/ml, 10 mg/ml, and 10 mg/ml of P25 TiO_2 (right); **(b)** comparing dispersions of sample 4-4-32 (left) and sample 4-9-27 (right), the concentrations of both dispersions are 10 mg/ml.

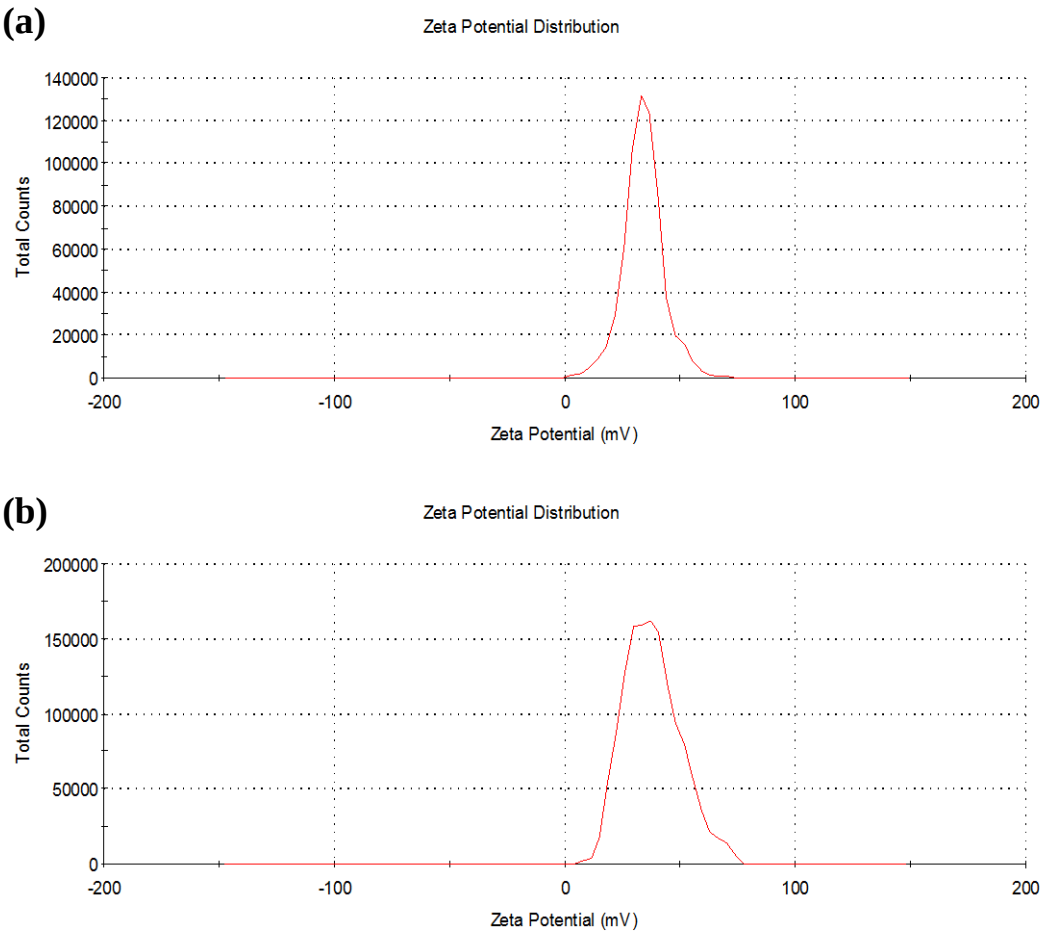

Figure 3.7 Zeta potential results of **(a)** sample 4-4-32; **(b)** sample 4-9-27.

In order to examine the thermal behavior of the synthesized TiO_2 nanoparticles to further improve the performance of hybrid electronic devices, DTA/TG in air was conducted. As shown in **Figure 3.8**, significant weight losses of the TiO_2 nanoparticle sample were detected starting from room temperature and an obvious endothermic peak was observed. The weight loss at temperatures lower than around 150 ℃ could be owing to the evaporation of remaining solvents used in synthesis process, i.e. H_2O and IPA (H_2O should be the major part). The further weight losses with the rising temperature could be ascribed to the removal of organic and/or chlorine residues and

the release of hydroxyl groups between nanoparticles or attached on the surface of TiO_2 nanoparticles (i.e. the Ti-OH). No weight loss was detected as the temperature rose above 600 ℃; the remaining weight of about 65 wt% was the weight of solid TiO_2 without impurity.

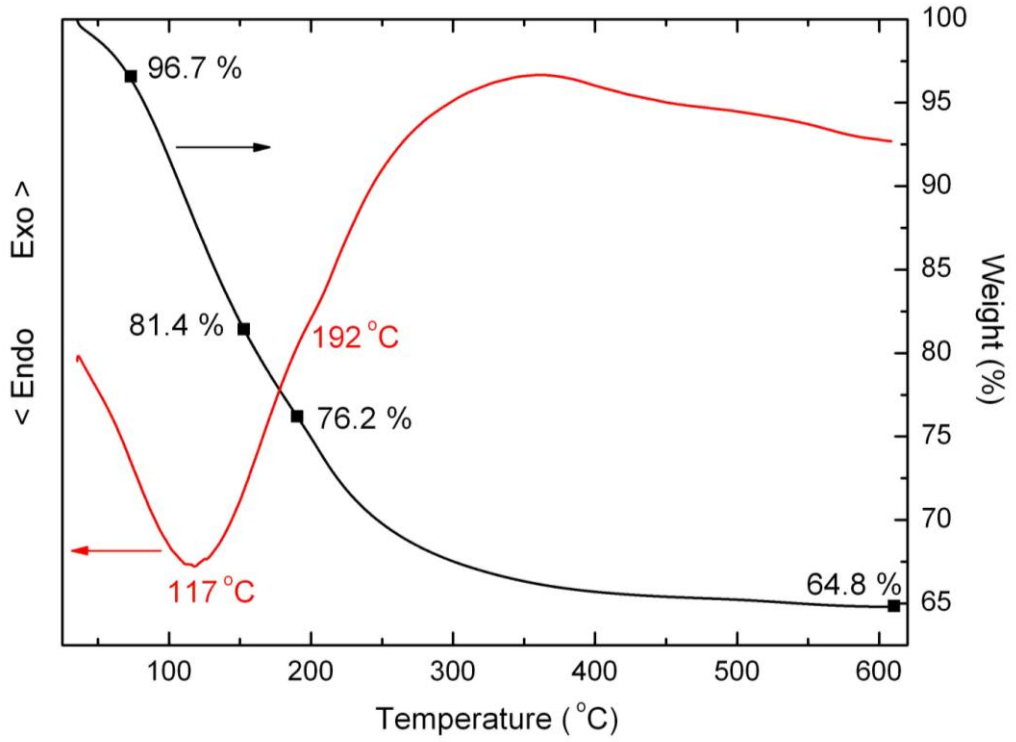

Figure 3.8 Thermal analysis of synthesized TiO_2 nanoparticle sample (4-4-32).

Figure 3.9 reports the FT-IR spectra of as-synthesized TiO_2 nanoparticles used in this study (sample 4-4-32) and P25 TiO_2. In the spectrum of as-synthesized TiO_2, the peak at 1618 cm^{-1} is due to the O–H in-plane bending (δ(O–H)) of adsorbed water molecules, which is the evidence of a certain amount of water present in the sample. The broad adsorption band with its peak at 3118 cm^{-1} corresponds to O–H stretching vibrations (ν(O–H)). The shoulder of this broad absorption band at around 3300 cm^{-1}

is attributed to the water molecules physically adsorbed within the sample, while the major part of the band at smaller wavenumbers is attributed to the hydroxyl groups attached on different sites of TiO_2 surface and to varying interactions between hydroxyl groups on TiO_2 [3]. The IR adsorption of as-synthesized TiO_2 is contrary to that of P25 TiO_2. In the P25 sample there is no detectable adsorbed water. The IR spectrum of the P25 TiO_2 specimen shows only noise signals due to the background subtraction [4] which is observed in both TiO_2 samples. From the results of FT-IR analysis, the major content besides the solid TiO_2 in our as-synthesized nanoparticles is the hydroxyl groups that could be removed with further thermal treatment as shown in the results of TG/DTA (**Figure 3.8**).

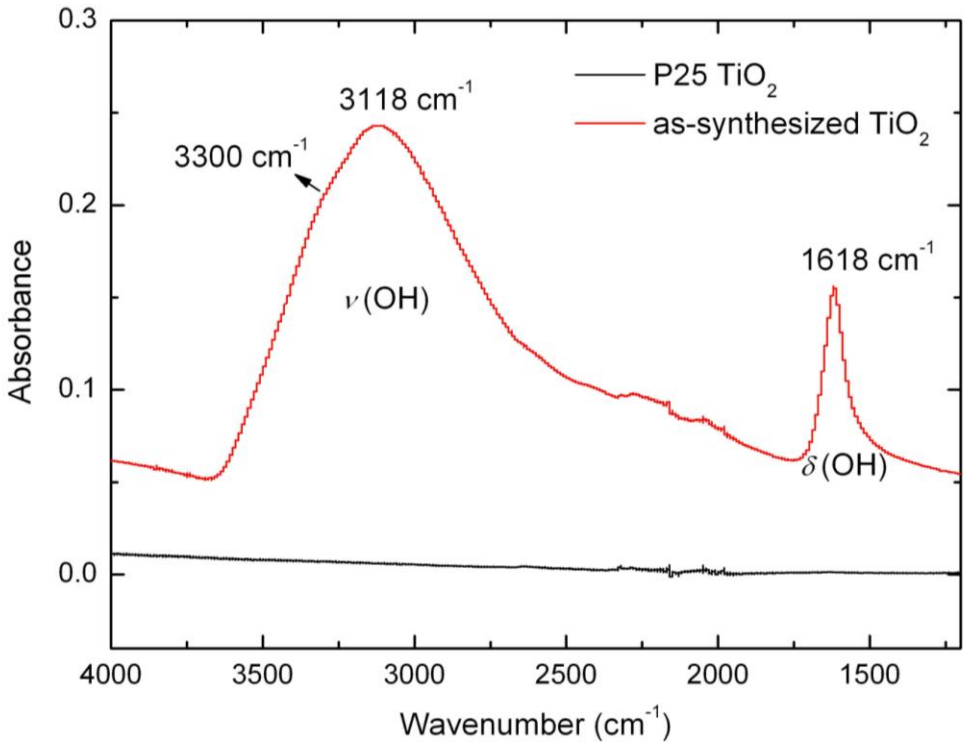

Figure 3.9 FT-IR spectra of the as-synthesized TiO_2 nanoparticle sample (4-4-32) and the P25 TiO_2.

3.3.2 Improving the performance of TiO_2/polymer LED with post-annealing

With the characterization and understanding of the synthesized TiO_2 nanoparticles, the largely attached hydroxyl groups on the surface of particles suggests a not compact microstructure of TiO_2 thin films deposited by spin-coating of nanoparticle dispersion. XPS was performed to examine the content of hydroxyl group exists in the as-deposited films. **Figure 3.10** shows the high-resolution XPS spectra of the Ti 2p and the O1s peaks taken on the surface of deposited TiO_2 thin film after UV-ozone exposure. The shape of the Ti 2p 3/2 peak at 459.0 eV is symmetric, which proves Ti^{4+} to be the only oxidation state in our TiO_2 material. This reinforces the distinction between our TiO_2 thin films and amorphous TiO_x films, which contain a substantial amount of coordinatively unsaturated Ti species (e. g. Ti^{3+}) in the films [5,6]. The O 1s peak is deconvoluted into two individual subpeaks: metal oxide (O^{2-}) and hydroxyl group (OH^-). The resulting peak positions for the O^{2-} and OH^- peaks are in good agreement with values reported by other studies [7,8]. The observed O^{2-} is assigned to the Ti-O bonding in bulk TiO_2 while the hydroxyl group is ascribed to the Ti-OH bonding on the surface of TiO_2 nanoparticles. The hydroxyl content of our TiO_2 materials is greater than other TiO_2 nanoparticles (e. g. P25 [9]) owing to the much larger surface area of the characteristically small nanoparticles (~ 2 nm).

The ratio of total amount of oxygen (OH^- plus O^{2-}, the oxygen amount related to the contamination of carbon was subtracted) to the contained Ti was calculated around 2.3, which means one Ti atom could have more than two oxygen atoms, and the excess oxygen was owing to the hydroxyl groups attached on particle surface. The number of O/Ti is close to the assumption that each of the outer Ti atoms on the surface of nanoparticles sized around 2 nm was attached by one OH^-. Assuming the shape of nanoparticles was similar as a sphere, the diameter of these spheres was

around 2 ± 0.4 nm, which could be imaged as 5 ~ 7 TiO_2 molecules in the length of diameter (the volume/molecule = 32.2 $Å^3$ for rutile, and 34.1 $Å^3$ for anatase), thus the molecules inside one nanoparticle, the numbers of outer TiO_2 with one hydroxyl group attached and the numbers of inner TiO_2 molecules with only (Ti-O-Ti) bonding are shown in **Table 3.1**.

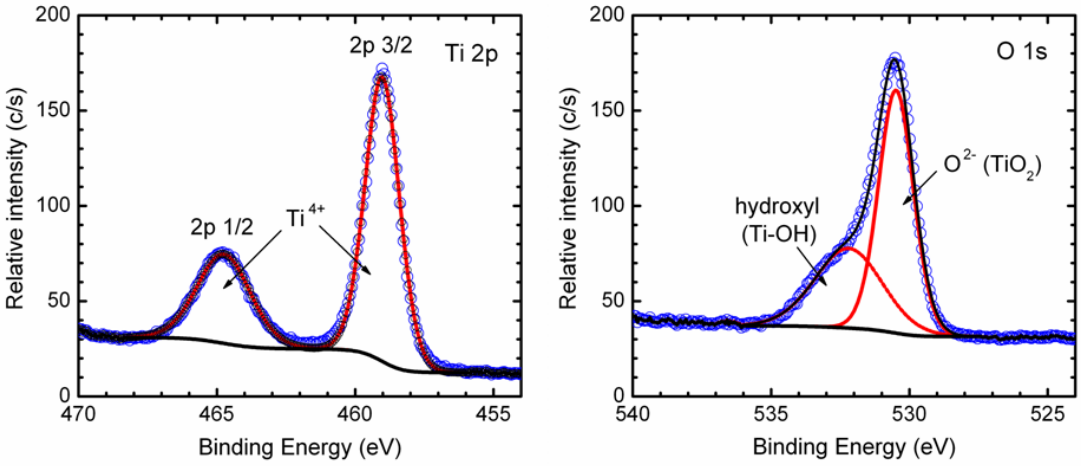

Figure 3.10 XPS spectra (Ti 2p and O1s) of the deposited TiO_2 thin film after treated with UV-ozone exposure.

Table 3.1 Sketched calculation for O/Ti ratio due to the attachment of OH^- on the outer layer (surface) of TiO_2 nanoparticles.

	Length of diameter = **5** TiO_2 molecules	Length of diameter = **6** TiO_2 molecules	Length of diameter = **7** TiO_2 molecules
Molecules in one nanoparticle	66	113	180
Number of **inner** TiO_2 molecules	15	38	66
Number of **outer** TiO_2 molecules	51	75	114
Extra O due to the attachment of OH^-	~ 13 (51/4)	~ 19 (75/4)	~ 29 (114/4)
Oxygen / Titanium (O/Ti ratio)	(13 + 66 × 2)/66 = 2.20	(19 + 113 × 2 /113 = 2.17	(29 + 180 × 2)/180 = 2.16

Therefore, to further ameliorate the performance of TiO_2/polymer hybrid LED, the hydroxyl groups surrounding the particle should be removed to render a better contact between TiO_2 nanoparticles. Since the XPS examination was carried out under a vacuum environment, most of detected hydroxyl groups should not be the physically absorbed water between nanoparticles due to the large interface area; the hydroxyls inside the TiO_2 films should be the chemically absorbed OH^- combining with Ti metal ion. Therefore, in order to massively remove hydroxyl groups, efficient thermal treatment has to be induced.

In this study, we adopted post-annealing process after the deposition of light-emitting polymer thin films. The stability of polymer materials while thermal treating at elevated temperatures is the key of successful post-annealing. **Figure 3.11** shows the DSC results of semiconducting F8BT copolymer used in this study, from the data measured, no decomposition reaction occurred at 300 ℃. The TGA data (**Figure 3.12**) provided by ADS Inc. also show no observable weight loss at temperatures lower than 300 ℃. From the thermal analyses of applied F8BT copolymer, 300 ℃ could be chosen as the working temperature for post-annealing treatment.

Figure 3.13 shows the current vs. voltage (I-V) and luminance vs. voltage characteristics of the TiO_2/polymer hybrid LEDs with a structure of ITO/TiO_2/Al_2O_3/F8BT copolymer/ MoO_3/Au. The LED fabricated with post-annealed hybrid layers turned on at ~ 6 V and reaches 100 cd/m^2 at ~ 7.5V. The maximum brightness of annealed hybrid LED approaches ~ 7000 cd/m^2 at 11.5 V. Comparing to the hybrid LEDs with the same device structure, the performance of annealed hybrid LED is apparently better than the hybrid LED without post-annealing. The maximum current efficiency at 100-200 mA/cm^2 is higher than 2 cd/A (**Figure 3.14**). This value

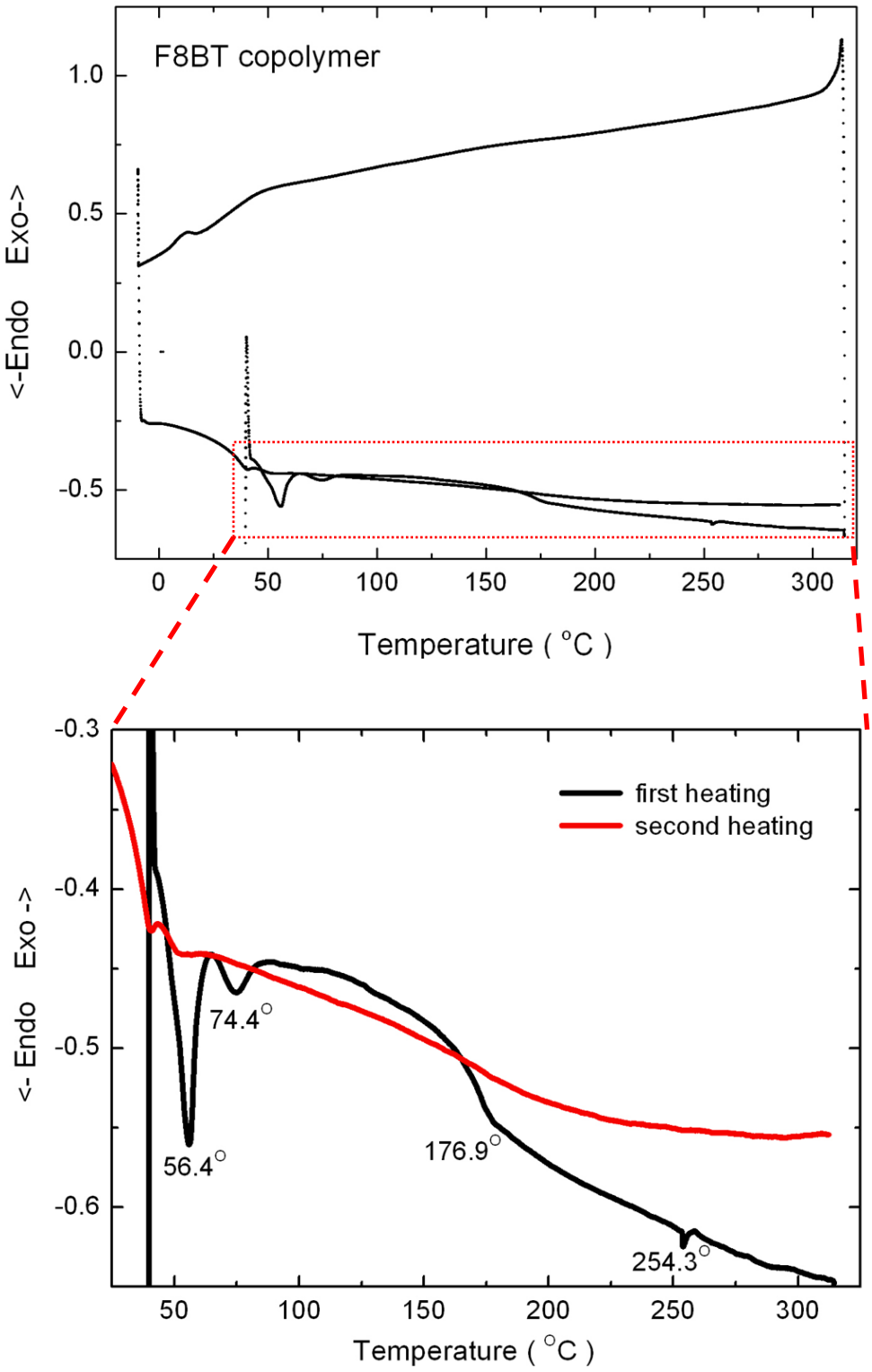

Figure 3.11 DSC analysis of F8BT copolymer: two heat/cool cycles (upper plot); detailed heating process (lower plot).

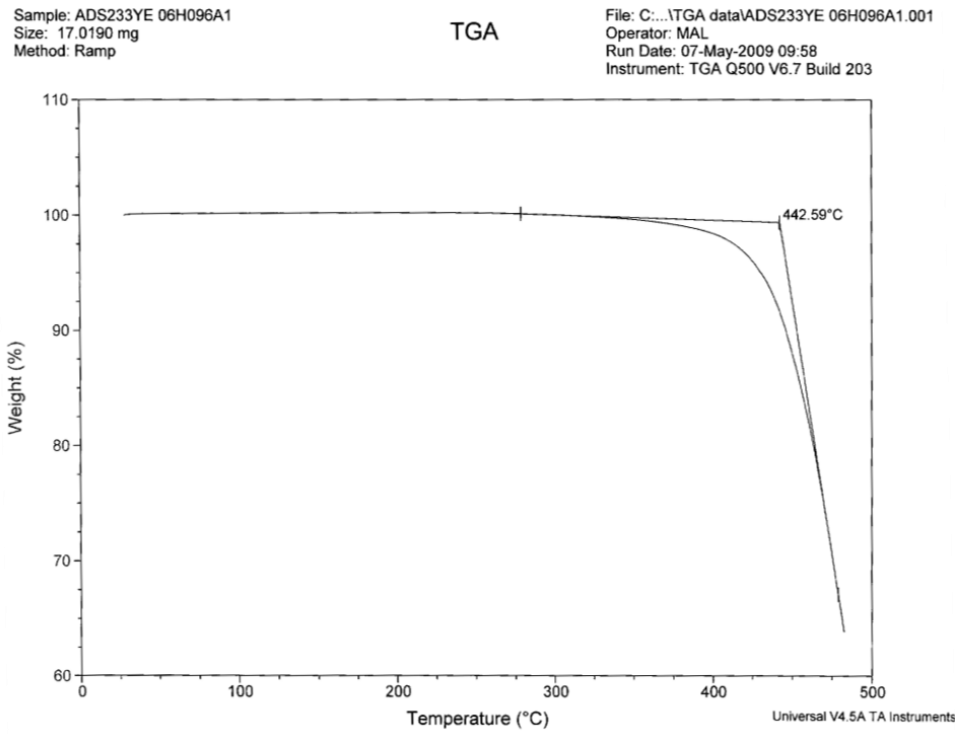

Figure 3.12 TGA analysis of F8BT copolymer (provided by ADS Inc.).

is three times higher than the performance of device (~ 0.6 cd/A) without post-annealing. The maximum luminous efficiency of our hybrid LED reached as high as 0.6 lm/W. To the best of our knowledge, the max brightness and efficiencies reported in this study present the best records in the literature for the performance of hybrid TiO_2/F8BT copolymer LEDs [10-12], and are comparable to the ZnO/F8BT copolymer hybrid LEDs [12,13].

Cross-section micrographs of TiO_2 thin film spin-coated on ITO coated glass substrate, F8BT copolymer deposited on top of TiO_2 thin film, and TiO_2/F8BT bilayer annealed at 300 ℃ for 2 hours were examined by FESEM (**Figure 3.15**). The FESEM images show that the thicknesses of both TiO_2 and F8BT layers were reduced after thermal annealing; the thicknesses of these layers before and after annealing are

compared in **Table 3.2**.

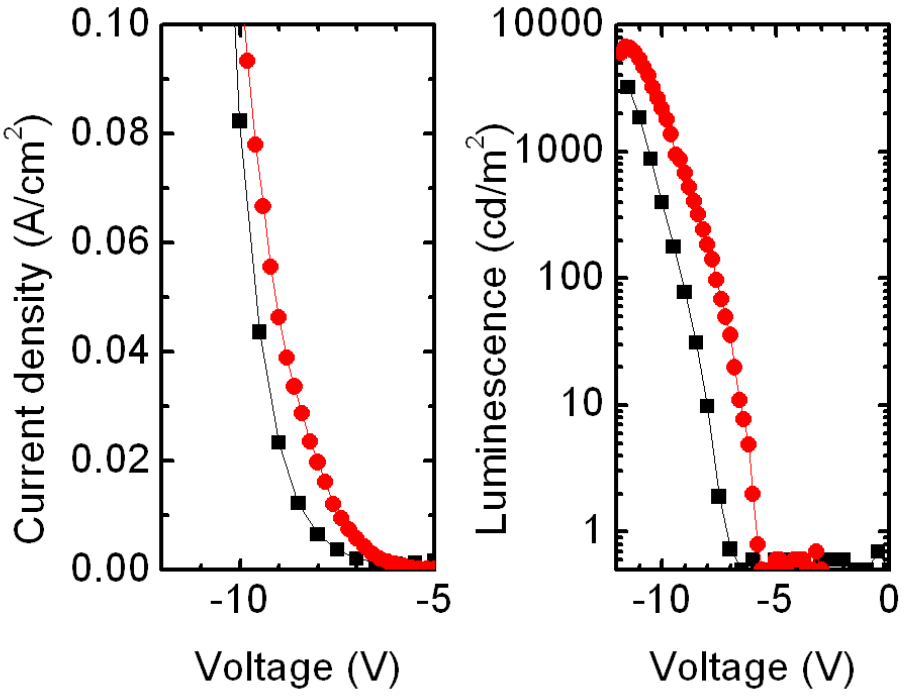

Figure 3.13 Current vs. voltage (J-V) and luminance vs. voltage (L-V) characteristics of TiO_2/polymer hybrid LEDs with the structure of ITO/TiO_2/Al_2O_3/F8BT copolymer/WO_3/Au. Data from two devices are shown: without post-annealing (squares ■) and one with post-annealing at 300 ℃ for 2 hours (circles ●).

The thickness of TiO_2 thin film was reduced around 20% after annealing, which suggests a densification of TiO_2 layer due to the removal of hydroxyl groups. On the other hand, the thickness of F8BT copolymer layer also decreased 20% after heating. To investigate the phenomenon of thickness reduction of polymer layer, a control measurement was carried out to heat F8BT copolymer deposited on Si wafer substrate with the same conditions (300 ℃, 2 hours) as the post-annealing applied in this study. It was observed that the thickness of F8BT layer was reduced about 10% after heating, and this phenomenon could be attributed to the re-arrangement of polymer molecules

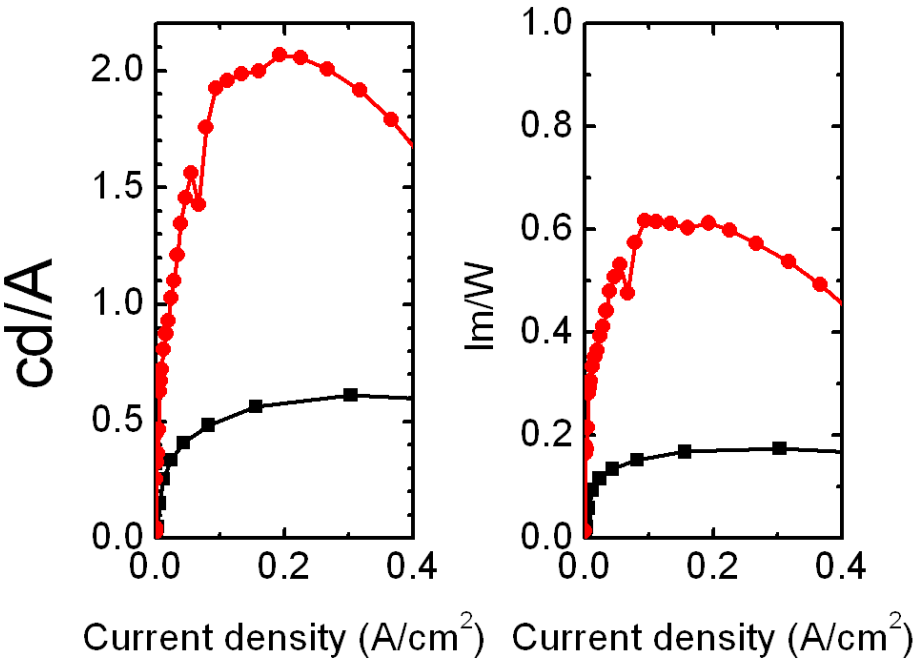

Figure 3.14 Current efficiency (left) and luminous efficiency (right) of TiO_2/polymer hybrid LEDs with the structure of ITO/TiO_2/Al_2O_3/F8BT copolymer/WO_3/Au. Data from two devices are shown: without post-annealing (squares ■) and one with post-annealing at 300 ℃ for 2 hours (circles ●).

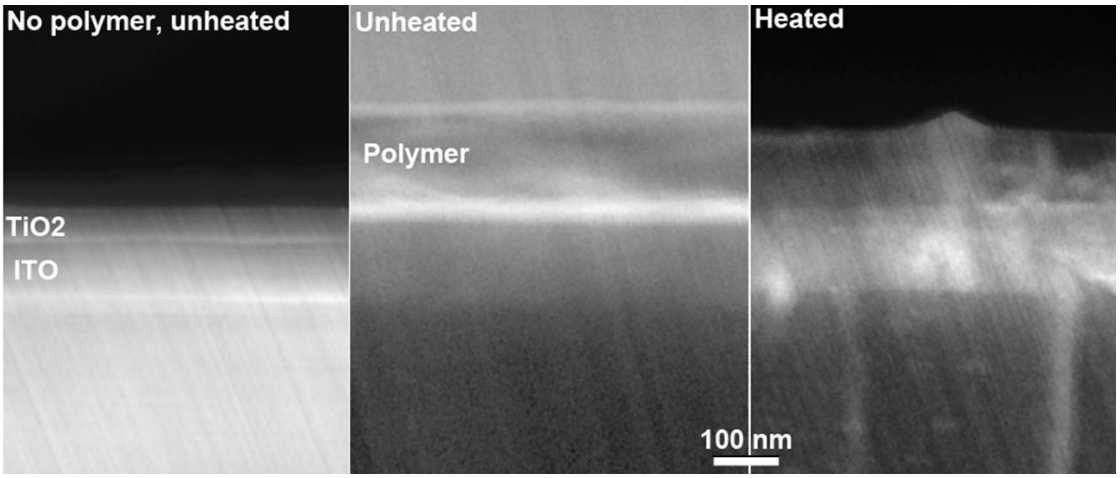

Figure 3.15 Cross-section micrograph of as-deposited TiO_2 thin film on ITO glass substrate (left), F8BT copolymer layer spin-coated on TiO_2 thin film (middle), and TiO_2/F8BT bilayer after 300 ℃ for 2 hours annealing (right).

Table 3.2 Thickness comparison of TiO_2 and F8BT layers.

	Before annealing	After annealing	Difference
TiO_2 thin film	50 nm	40 nm	10 nm (20 %)
F8BT copolymer	150 nm	120 nm	30 nm (20%)

that made a denser configuration of the F8BT copolymer layer. Thus, the thickness difference of F8BT layer used in our hybrid LED devices should be only 15 nm after post-annealing. However, a much larger thickness decrease (~ 30 nm) was observed for the F8BT in the TiO_2/F8BT bilayer that suggests a penetration of polymer into the porous TiO_2 layer.

To further demonstrate the penetration of F8BT copolymer into the bottom TiO_2 film, SIMS was conducted to determine the depth profiles of TiO_2 thin film as well as the TiO_2/F8BT bilayer before and after annealing. **Figure 3.16** illustrates the depth profiles of constituent species for TiO_2/F8BT bilayer. It was confirmed that both thicknesses of the F8BT copolymer layer and the bottom TiO_2 film were reduced after annealing, and the thickness of bottom TiO_2 film reduced around 80 %, which further proves the results obtained from the cross-section micrographs. The two depth profiles of carbon before and after annealing indicate that carbon content inside the TiO_2 thin films increased significantly just after annealing. The observed phenomenon of carbon increasing is reasonably attributed to the diffusion of polymer molecules from F8BT copolymer layer into the bottom TiO_2 film.

However, as shown in **Figure 3.17**, the thickness of bare TiO_2 thin film reduced up to around 37 % after annealing, which was almost the double of the thickness

reduction ratio of TiO_2 film in TiO_2/F8BT copolymer bilayer. From the observation above, without the deposition of top polymer layer – i.e. without the diffusion of polymer, the TiO_2 films could be further densified after thermal annealing.

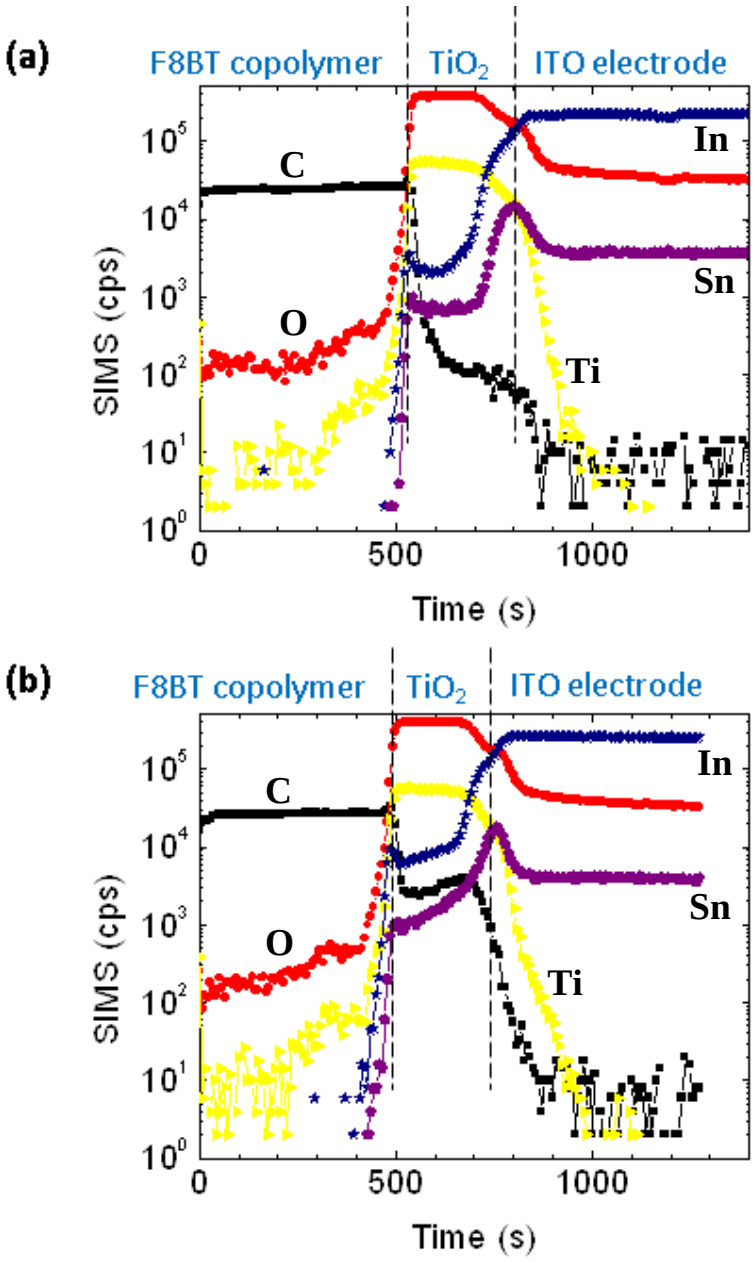

Figure 3.16 SIMS profiles of TiO_2/F8BT copolymer bilayer deposited layer by layer on top of ITO electrode, **(a)** before 300 ℃ annealing for 2 hours; **(b)** after 300 ℃ annealing for 2 hours.

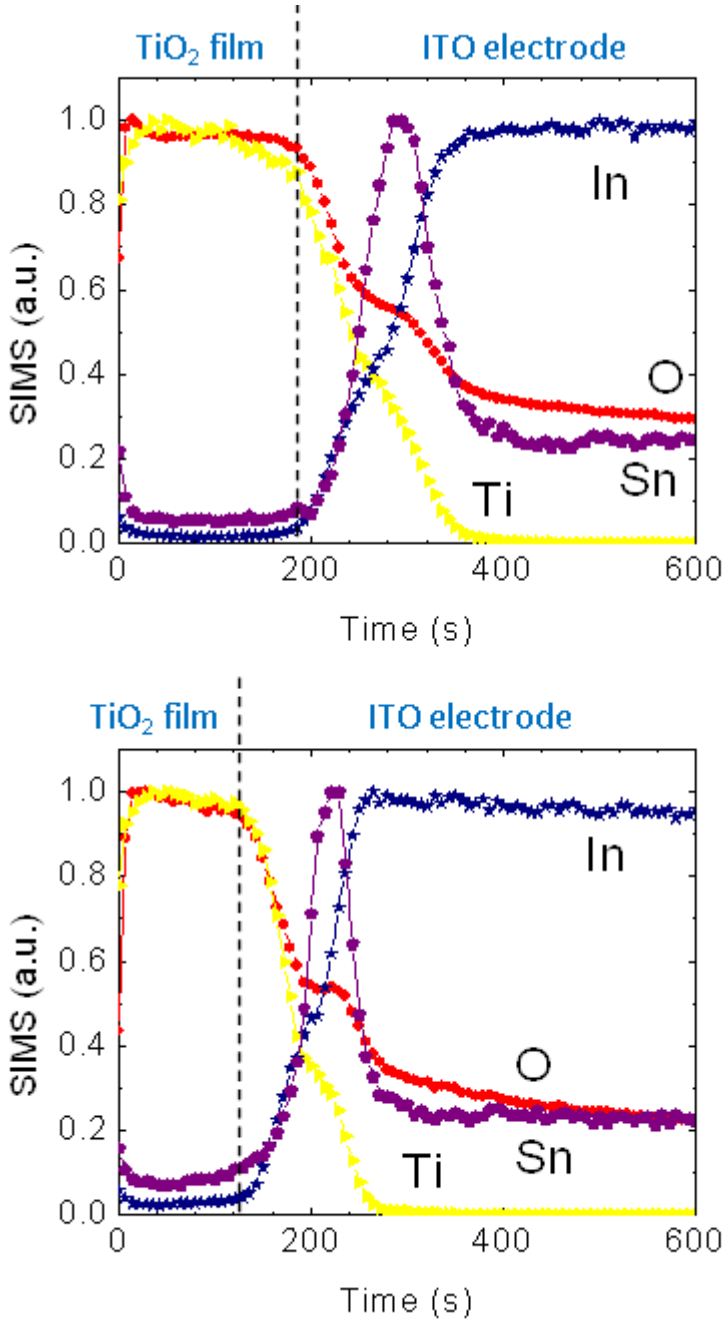

Figure 3.17 SIMS profiles of TiO_2 thin film deposited on top of ITO substrate, **(a)** before 300 ℃ annealing for 2 hours; **(b)** after 300 ℃ annealing for 2 hours.

The SIMS results and the micrographs suggest that the microstructure of bottom TiO_2 thin film was not compact and the porosity of it could be derived from the

amount of polymer on top diffused into the TiO_2 film. Since there was a 15 nm (total decreased thickness – thickness decreased due to the polymer re-arrangement, 30 nm – 15 nm) extra decrease in thickness of the top polymer layer after annealing, the porosity of bottom 40 nm thick TiO_2 layer could be estimated as:

porosity (%) = (15/40) = 37.5 % (Equation 3.1)

The calculation result suggests that with the deposition of top polymer layer, a more porous microstructure of TiO_2 film was formed after post annealing. Another way to prove the conclusion above is to consider the volume contraction of TiO_2 film due to the removing of hydroxyl groups. Equation 3.2 below estimates the thickness decrease of TiO_2 film after thermal annealing according to the conservation of total volume of no OH^- attached TiO_2 nanoparticles. The contraction ratio of each dimension of bulk TiO_2 was calculated using the radial contraction ratio of TiO_2 nanoparticles after removing the adsorbed hydroxyl groups on the particle surface (the length of hydrogen bond between two TiO_2 nanoparticles is estimated around 0.3 nm [14]). Since no shrinkage of TiO_2 thin films was observed along directions parallel to the ITO substrates (i.e. no area shrinkage), the film thickness of TiO_2 should be reduced more than 34 % after post annealing. The result of SIMS analysis (**Figure 3.17**) consists with the derivation of Equation 3.2 that more reduction of the thickness of TiO_2 layer was observed, and the microstructure of bare TiO_2 film was definitely more compacted than that in TiO_2/F8BT copolymer bilayer which only reduced ~ 20 % in thickness after post annealing.

Volume contraction of TiO_2 film = $(2 \text{ nm}/2.3 \text{ nm})^3$ = 65.8 %

= (1 – area shrinkage) × (1 – thickness reduction)

⇨ Reduction of film thickness = 34.2 % (Equation 3.2)

The more porous microstructure could be attributed to the penetration of polymer into the bottom layer that prevented the further contraction of TiO_2 thin films. Moreover, as the contraction of TiO_2 film in directions parallel to ITO substrates was restricted, as shown in **Figure 3.18**, the restricted contraction could be considered as stresses applying in opposite directions that pull apart the TiO_2 layer and then made more polymer molecules diffuse in.

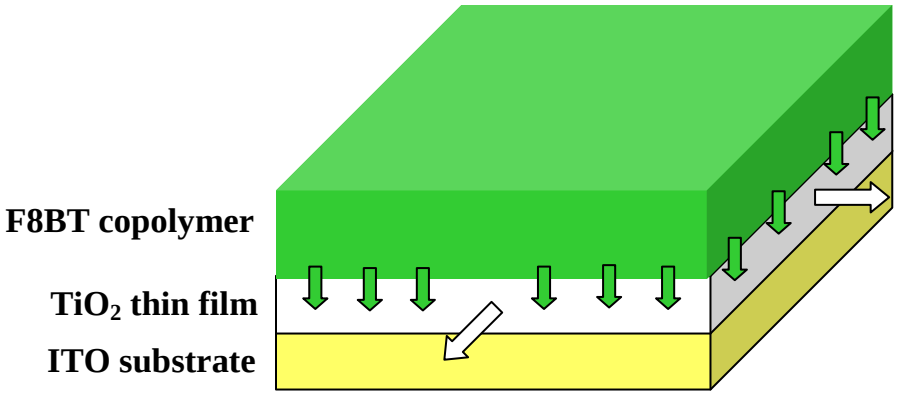

Figure 3.18 Schematic plot showing the diffusion of F8BT copolymer into a less compact TiO_2 thin film as conducting post annealing.

The whole picture of TiO_2/F8BT copolymer bilayer undergoing post-annealing as well as the ins and outs of improved device performance are illustrated in the microstructure model presented in **Figure 3.19.**

With the post annealing after the deposition of F8BT copolymer on top of TiO_2 thin films consisted by nanoparticles synthesized in this study, the OH^- attached on the surface of TiO_2 nanoparticle were removed to make a better contact between nanoparticles. Moreover, the diffusion of F8BT copolymer into the TiO_2 thin films

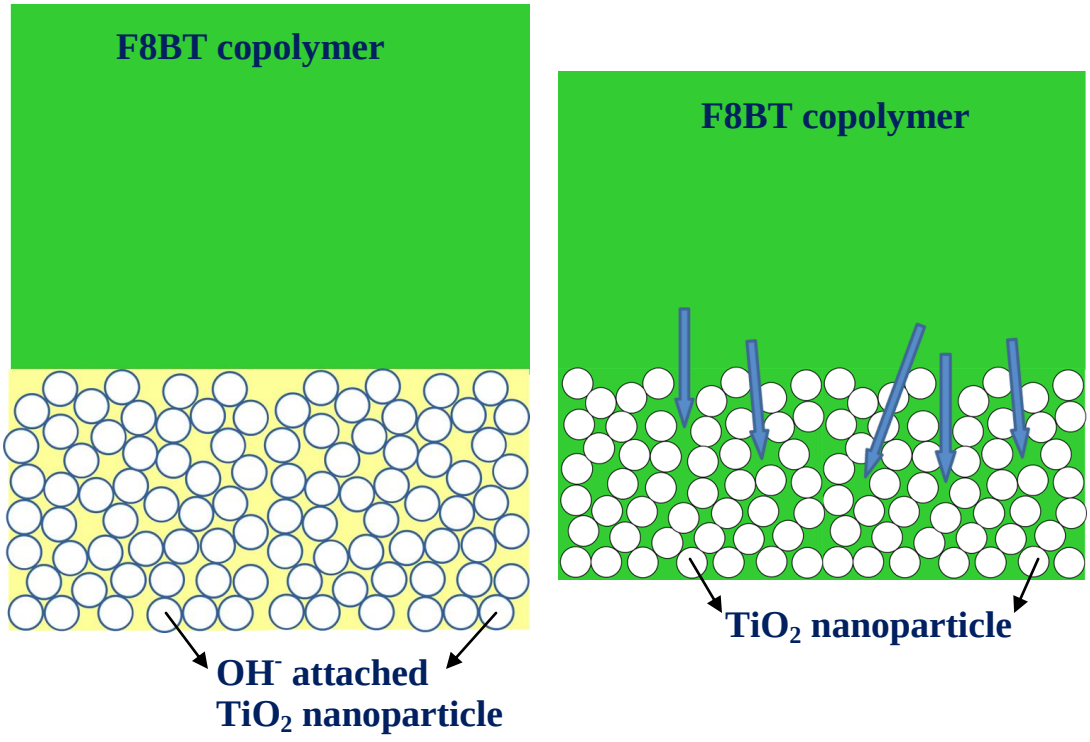

Figure 3.19 Microstructure models of TiO_2/F8BT copolymer bilayer, before 300 ℃ annealing for 2 hours (left); after 300 ℃ annealing for 2 hours (right).

could prevent further coherence of nanoparticles due to the annealing and a more porous TiO_2 film penetrated with polymer was form. Novel bulk heterojunction of electron-transporting TiO_2 and light-emitting polymer was obtained due to the nanoscale blending and a very large interconnection area formed after post annealing. With the outstanding performance of TiO_2/F8BT hybrid LED obtained in this study, an ingenious process that improves the performance of inorganic/organic hybrid devices was demonstrated.

Conclusion

In summary, with the characterizations of as-synthesized TiO_2 nanoparticles, a

certain amount of hydroxyl groups were proved adsorbed around the 2 nm-sized TiO_2 nanoparticles. Post-annealing of TiO_2/F8BT copolymer bilayer could remove the adsorbed hydroxyl groups in the bottom TiO_2 while also made the F8BT copolymer diffuse into the TiO_2 layer. Bulk heterojunction of electron-transporting TiO_2 and light-emitting polymer was formed after post-annealing and the performance of TiO_2/F8BT copolymer hybrid LEDs was largely improved. TiO_2/F8BT hybrid LEDs show a promising brightness ~ 7000 cd/m^2 and an outstanding current efficiency as high as 2 cd/A (as a record number of TiO_2/F8BT copolymer hybrid LEDs), which is three times higher than the efficiency of hybrid LEDs without the post-annealing treatment. With the results shown in this study, a novel process could be proposed to fabricate advanced inorganic/polymer hybrid devices – deposit inorganic thin films with hydroxylated nanoparticles, and then post-anneal the inorganic/polymer bilayer to make the polymer diffuse into the inorganic layer and to form bulk heterojunction between inorganic/organic hybrid materials.

REFERENCES

[1] C. H. Wu, H. Li, H. H. Fong, V. A. Pozdin, L. A. Estroff, G. G. Malliaeas, Org. Electron. 12 (2011) 1073.

[2] W. Wang, B. H. Gu, L. Y. Liang, W. A. Hamilton, D. J. Wesolowski, J. Phys. Chem. B 108 (2004) 14789.

[3] T. Bezrodna, G. Puchkovska, V. Shymanovska, J. Baran, H. Ratajczak, J. Mol. Struct. 700 (2004) 175.

[4] Pouchert C.J., 1981. The Aldrich Library of Infrared Spectra. Aldrich Chemical Co, Milwaukee.

[5] K. Lee, J. Y. Kim, S. H. Park, S. H. Kim, S. Cho, A. J. Heeger, Adv. Mater. 19 (2007) 2445.

[6] D. Luca, D. Macovei, C.-M. Teodorescu, Surf. Sci. 600 (2006) 4342.

[7] E. McCafferty, J. P. Wightman, T. F. Cromer, J. Electrochem. Soc. 146 (1999) 2849.

[8] S. Hofman, J. M. Sanz, J. Trace Micro. Tech. 1 (1982/83) 213.

[9] B. Erdem, R. A. Hunsicker, G. W. Simmons, E. D. Sudol, V. L. Dimonie, M. S. El-Aasser, Langmuir 17 (2001) 2664.

[10] H. J. Bolink, E. Coronado, D. Repetto, M. Sessolo, E. M. Barea, J. Bisquert, G. Garcia-Belmonte, J. Prochazka, L. Kavan, Adv. Funct. Mater. 18 (2008) 145.

[11] S. A. Haque, S. Koops, N. Tokmoldin, J. R. Durrant, J. Huang, D. D. C. Bradley,

E. Palomares, Adv. Mater. 19 (2007) 683.

[12] D. Kabra, M. H. Song, B. Wenger, R. H. Friend, H. J. Snaith, Adv. Mater. 20 (2008) 3447.

[13] J. W. Ryan, E. Palomares, E. Martinez-Ferrero, J. Mater. Chem. 21 (2011) 4774.

[14] M. Chaplin, Water Structure and Science, http://www.lsbu.ac.uk/water/evidnc.html#rad (accessed 4/10/2011).

CHAPTER 4

FABRICATION OF THIN-FILM TRANSISTORS USING AMORPHOUS IGZO OXIDE SEMICONDUCTOR WITH SOLUTION DEPOSITION PROCESS

Introduction

In decades, there is always a rising demand for improving the performance and lowering the manufacture cost of thin film transistors (TFT), and the most efficient improvement can be achieved readily by replacing the materials of channel layer in TFTs. Lately, amorphous oxides have attracted considerable interest from the electronic industry for their application as semiconducting active layer in TFTs [1-8]. Among these oxide semiconductors, in particular, amorphous In-Ga-Zn-O oxide (a-IGZO) had been extensively investigated for the remarkable advantages such as: low processing temperature, large electron mobilities, low operation voltage, ease of fabrication, and large allowance in the choice of gate insulator etc. [9].

The majority of reports in the literature have demonstrated TFTs using high field-effect mobility (≥ 10 $cm^2/V \cdot sec$) a-IGZO films as the active layer, which were deposited typically by pulsed laser deposition (PLD) or rf sputtering process [4-6]. The disadvantage of these processes is that both of them require vacuum environment, and thus slow the fabrication of TFT devices as preparing the a-IGZO films while also limit large-scale manufacturing of related electronic devices. In light of the trend for fabricating large-scale and large-area integrated circuits, unambiguously, liquid phase deposition processes could be more promising due to the lower requirement for the conditions and much lower processing cost for large-scale fabrication.

More recently, several reports in the literature have demonstrated TFT using a-IGZO thin film as the channel layer, that were prepared by liquid phase deposition processes such as spin-coating [10-15] or printing [16] with sol-gel precursor solutions, and the starting materials for these sol-gel precursors were acetate, nitrate or chlorate-related ionic compounds. However, the complicated chemistry of the sol-gel process while the decomposition of organometallic precursors during annealing could cause the porous structure of a-IGZO thin films [17], and also the worry of residues of anions (e. g. Cl^-) in the a-IGZO thin films could be a potential problem that degrades the performance of fabricated TFTs.

In this work, we present a facile liquid phase process for the preparation of a-IGZO thin films via a metal–organic decomposition (MOD) method. The solution of metal acetylacetonates was adopted as the precursor, and the a-IGZO films were deposited by spin-coating. The deposited films were annealed at moderately low process temperature (≤ 500 ℃). The pyrolyzing behavior and the formation of a-IGZO were studied. The relationship between the composition of metal ion species and the device performance was also investigated. The prepared a-IGZO thin films were confirmed to possess promising electric properties suitable for the TFT usage.

Experimental

In the present study, top-contact bottom-gate transistors using a-IGZO as the metal oxide semiconducting channel were fabricated (as shown in **Scheme 4.1**). Heavily doped Si⟨100⟩ wafers were used as gate electrodes with a 200 nm thermally grown silicon dioxide layer as the gate dielectric. The substrates were cleaned by sonication

in semiconductor grade acetone and isopropyl alcohol for 10 minutes in each solvent. Prior to the deposition of a-IGZO thin films, pre-cleaned substrates were treated with a 10-minute UV-ozone (Jetlight) exposure.

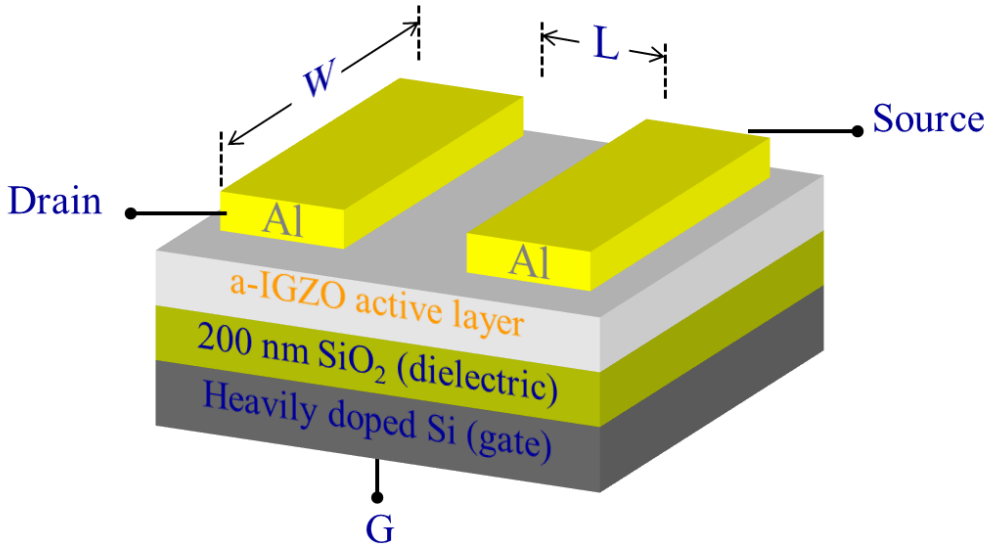

Scheme 4.1 Device with a bottom-gate TFT structure with an a-IGZO active layer.

The a-IGZO thin films were prepared via a metal-organic decomposition (MOD) method. All of the starting materials were purchased from Sigma-Aldrich Co. and used as received. The precursor solutions for MOD were obtained by mixing 0.05 M of gallium acetylacetonate [$Ga(C_5H_7O_2)_3$] ($Ga(acac)_3$, 99% pure), 0.05 M of zinc acetylacetonate hydrate [$Zn(C_5H_7O_2)_2 \cdot xH_2O$] ($Zn(acac)_2 \bullet xH_2O$, 99% pure) dissolved in ethanol and 0.05 M of indium acetylacetonate [$In(C_5H_7O_2)_3$] ($In(acac)_3$, 99% pure) dissolved in tetrahydrofuran (THF) at different volume ratios to render the varied molar ratios of In, Ga, and Zn needed for this study. Prior to film coating, the precursor solutions were stirred for 24 hours at room temperature in N2 atmosphere and then pre-heated at 65 ℃ before using. The prepared solutions were spin-coated onto the cleaned Si/SiO_2 substrates at a spinning rate of 6000 rpm. After coating, thin films with organic raw materials were pyrolyzed and annealed directly on a hot plate

in air at temperatures ranging from 340 ~ 500 ℃ for 2 hours to decompose the organic components. The typical thickness of a-IGZO films was measured around 10 nm by an ellipseometer. The surface morphology of the films was observed with an atomic force microscope (AFM, DI 3100 Dimension microscope) using tapping mode.

Thermogravimetric analyses (TGA) were performed to investigate the thermal behavior of the stoichiometric mixture of starting materials. The as-pyrolyzed films were identified amorphous phase by X-ray diffraction (XRD) using a Theta-Theta Diffractometer (Scintag Inc.) with Cu Kα1 radiation at 40 kV and 30 mA. The composition of as-pyrolyzed films was analysed by X-ray photoelectron spectroscopy (XPS, Surface Science Instruments SSX-100, monochromatic Al Kα; 1486.6 eV) at selected take-off angles (TOA).

Prior to electrical characterization, top drain and source aluminum contacts were deposited. These contacts were 60 nm thick and were thermally evaporated at a rate of 0.1 nm/sec through a metal shadow mask that defined a series of transistor devices with a channel length (L) of 100 μm and a channel width (W) of 1,800 μm. The electrical characterization was carried out using a four-point probe station under vacuum (10^{-6} torr) at room temperature. The field-effect mobility μ_{FE} was extracted both from the saturation and linear regimes. The drain-source current (I_{DS}) was measured vs. the drain-source voltage (V_{DS}) using the Lakeshore probe station and Keithley 4200-SCS Semiconductor Characterization System. The mobility (μ_i) was evaluated using the following equation:

$$I_{DS,sat} = \frac{W}{2L} \mu_i C_r (V_{GS} - V_{TH})^2 \qquad \text{(Equation 3.1)}$$

where C_r is the capacitance per unit area of the gate dielectric layer, and V_{TH} is the threshold voltage. V_{TH} was determined from the intercept in the plot of $(I_{DS})^{1/2}$ vs V_{GS}.

Results and Discussion

Thermal behaviour of the starting materials was investigated by TGA. All three starting materials and the mixture with stoichiometry of a-IGZO (In:Ga:Zn = 1:1:1) were heated to 600 ℃ at a rate of 10 ℃/min in standard air atmosphere. As shown in **Figure 4.1**, significant weight losses of $In(acac)_3$ and $Ga(acac)_3$ were observed starting around 200 ℃, while the weight of $Zn(acac)_2 \bullet xH_2O$ started to sharply decrease at around 150 ℃ after the removing of hydrated water at around 100 ℃. Because all of the remaining weights of these starting materials after heating are less than the predicted weights of oxide products (i.e. In_2O_3, Ga_2O_3 and ZnO) obtained after decomposition reactions, evaporation of these metal acetylacetonates should occur with the rising of temperature.

From the phenomenon described above, to reduce the evaporation of starting materials as preparing a-IGZO thin films, the precursors on substrates should be annealed with a higher rate of temperature increasing. In this study, the as-deposited films were annealed in air via two types of heating processes. The first method was to anneal the films from room temperature at a slow heating rate of 5 ℃/min. The second method was to anneal the precursor films directly on a "hot" hotplate with the set temperatures to make a rapid temperature rising. Both processes were to heat the precursor films for two hours at setting temperatures. The crystal phases present in the as-annealed thin films were examined by XRD. After annealing in air for 2 hours at temperatures within our operation window (340 to 500 ℃), all of the obtained IGZO

thin films were confirmed to be amorphous.

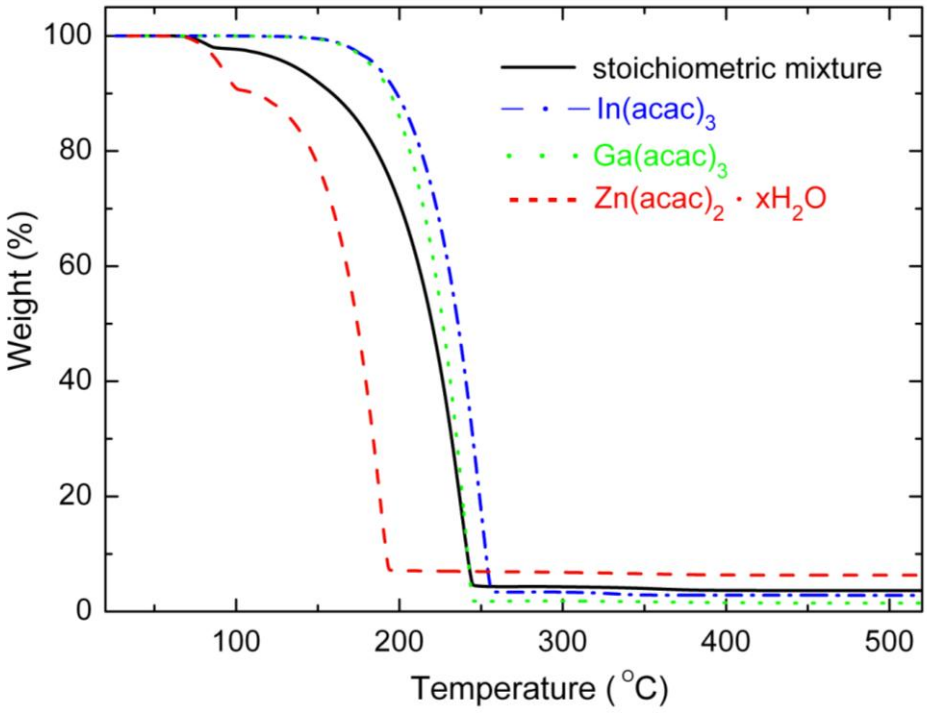

Figure 4.1 TGA results of starting materials used in this MOD process. The analyzed powder samples include In, Ga, Zn acetylacetonates and the In:Ga:Zn = 1:1:1 stoichiometric mixture.

The surface morphology of a-IGZO thin films annealed at 500 ℃ via the slow and rapid heating was examined via AFM. As shown in **Figure 4.2**, Flat and smooth surface could be obtained with the slower heating rate, the RMS roughness of the smoother film (over a scan area of 1 μm x 1 μm) was only 0.48 nm. The film heated directly on the hot plate show was essentially flat (RMS ~ 0.9 nm) but with poles around 10 nm heights distributed over the surface of the films. The formation of these poles could be due to the sudden sublimation of starting materials before decomposition. After further examination of the device performance of annealed a-IGZO films, the quick heated films behave similar or sometimes better to the slow

heated device, which could be attributed to the easier control of the element composition of the films. Thus in this study, the a-IGZO thin films prepared for TFT device fabrication were heated by the direct heating process.

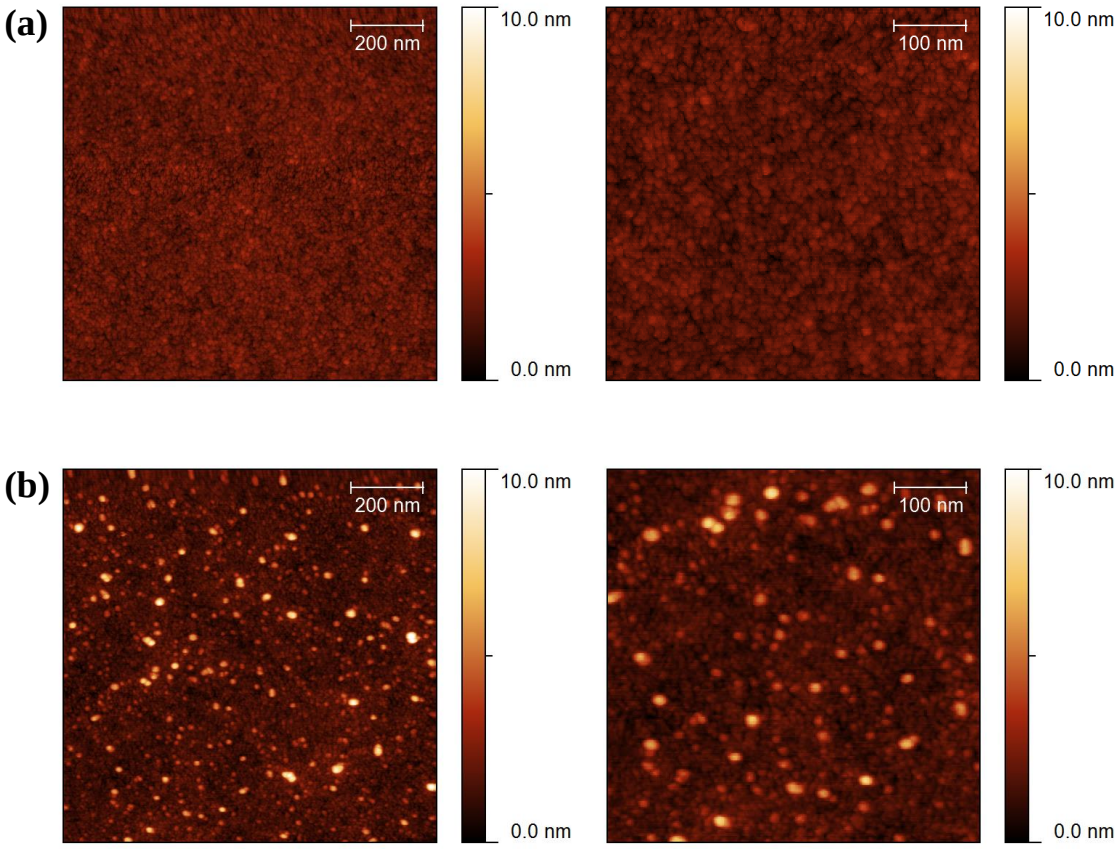

Figure 4.2 AFM images for a-IGZO films annealed at 500 ℃ via the slow heating **(a)**, and rapid heating **(b)**.

Figure 4.3 shows the transfer characteristics of four IGZO transistors (In:Ga:Zn = 1:1:1), which is prepared by fast annealing from 386-500 °C for 2 hours in ambient environment. The corresponding saturation mobility and the threshold voltage are extracted according to **Figure 4.3** and summarized in **Figure 4.4**. At 386 °C, the

deduced onset voltage appears to be positively shifted to ~20 V. Under higher temperature annealing, V_{on} shifts to zero. At annealing temperature of 500 °C, V_{on} further shifts negatively to -32 V. It is obvious that the 1:1:1 IGZO film operates at enhancement mode with lower annealing temperatures and converts to depletion mode with higher annealing temperatures. **Figure 4.4** shows the corresponding saturation mobility and the device threshold voltage V_{TH} of a-IGZO film extracted from **Figure 4.3**. The annealing process of a-IGZO formation can be catalogued into 2 regions: a) decomposition of precursors at low annealing temperature and, (b) formation of oxygen vacancies that largely increases the mobility of a-IGZO film at higher annealing temperatures.

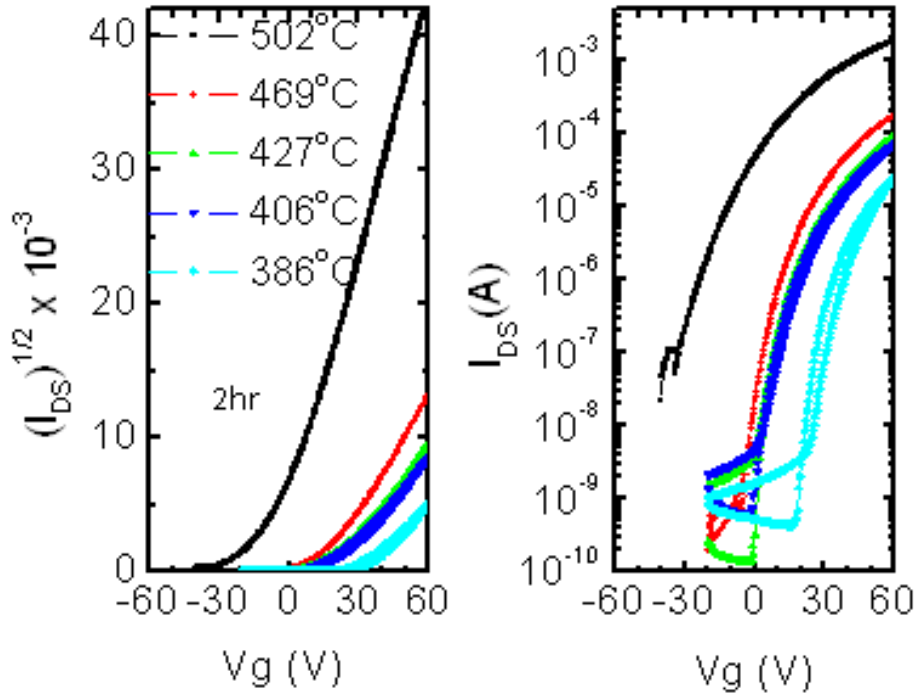

Figure 4.3 Drain current (I_{DS}) vs. gate voltage (Vg) transfer curves of TFTs with a-IGZO active layers annealed at different temperatures for 2 hours.

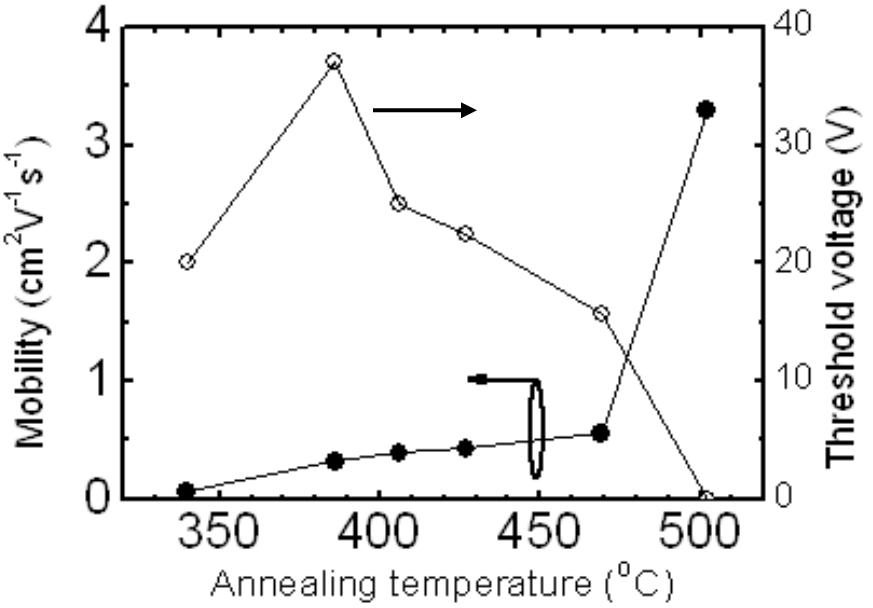

Figure 4.4 The mobilities and threshold voltages (V_{TH}) of TFTs with a-IGZO active layers annealed at different temperatures for 2 hours.

The a-IGZO film annealed at low temperature (340 °C, 2 hours) shows a typical transistor characters and exhibits a field effect mobility of 0.06 $cm^2V^{-1}s^{-1}$ with a V_{TH} of 20V. It is likely that the decomposed precursors were converted into a-IGZO directly under low temperature annealing. Upon further increasing of the annealing temperature from 386-469°C, the mobility gradually increases from 0.32 to 0.56 $cm^2V^{-1}s^{-1}$ while the corresponding V_{TH} rises up from 20 V to 37 V spanning the range of 340-386 °C and then decrease down to 15.7 V at 469 °C. This V_{TH} reduction suggests that the a-IGZO films approach to the fully oxidized condition at around 386 °C. The highest mobility of a-IGZO active layer obtained in this study is 3.4 $cm^2V^{-1}s^{-1}$ (500 °C, 2 hours) which shows the promising of our MOD process comparing to other solution preparations of a-IGZO films [17,18].

Table 4.1 The atomic ratio (%) of the a-IGZO films determined by XPS at TOA 35°

Temperature °C	In	Ga	Zn	O
340	21.3	3.5	10.6	64.6
400	20.6	3.5	7.9	67.9
450	19.4	3.2	7	70.5
500 (TOA 35°)	20	5.1	8.2	66.8
500 (TOA 90°)	16.7	6.2	8	65.9

Table 4.1 shows the composition of the a-IGZO films studied by the XPS (at TOA 35°) after thermal annealing (rapid heating) at various temperatures. It is interesting that the actual atomic ratio of In:Ga:Zn deviates from the ratio of the stoichiometric mixture of 1:1:1. Element In dominates the composition of the metal content of the a-IGZO films and the composition of In remains almost the same throughout the whole annealing temperature range. Both Zn and Ga concentrations are lower than the presumed concentrations of the a-IGZO precursor solutions. It is likely suggested that when annealing, Ga and Zn precursors sublimed from the spin-coated MOD film prior to fully oxidization to form the IGZO matrix. The XPS results of slow heated a-IGZO films also show a composition deviated from 1:1:1.

Figure 4.5a shows the representative XPS O 1s plot of a-IGZO annealed at 500 °C in air. In general, the O 1s peak is fitted by three peaks to evaluate their relative contributions to the oxygen state. The component on the low binding energy of O 1s XPS peak, labelled as O_I centred at 530 eV, is attributed to O^{2-} ions surrounded by In, Ga, and Zn atoms in the IGZO film, i.e. metal oxide. This O_I component is a measure of the amount of oxygen atoms in a fully oxidized stoichiometric environment. As shown in **Figure 4.5b**, O_I slightly decreases upon annealing at higher temperatures (> 400 °C), suggesting that the release of coordinated oxygen from the site to form oxygen vacancies (increase of O_{II}) under considerable thermal activation. The high

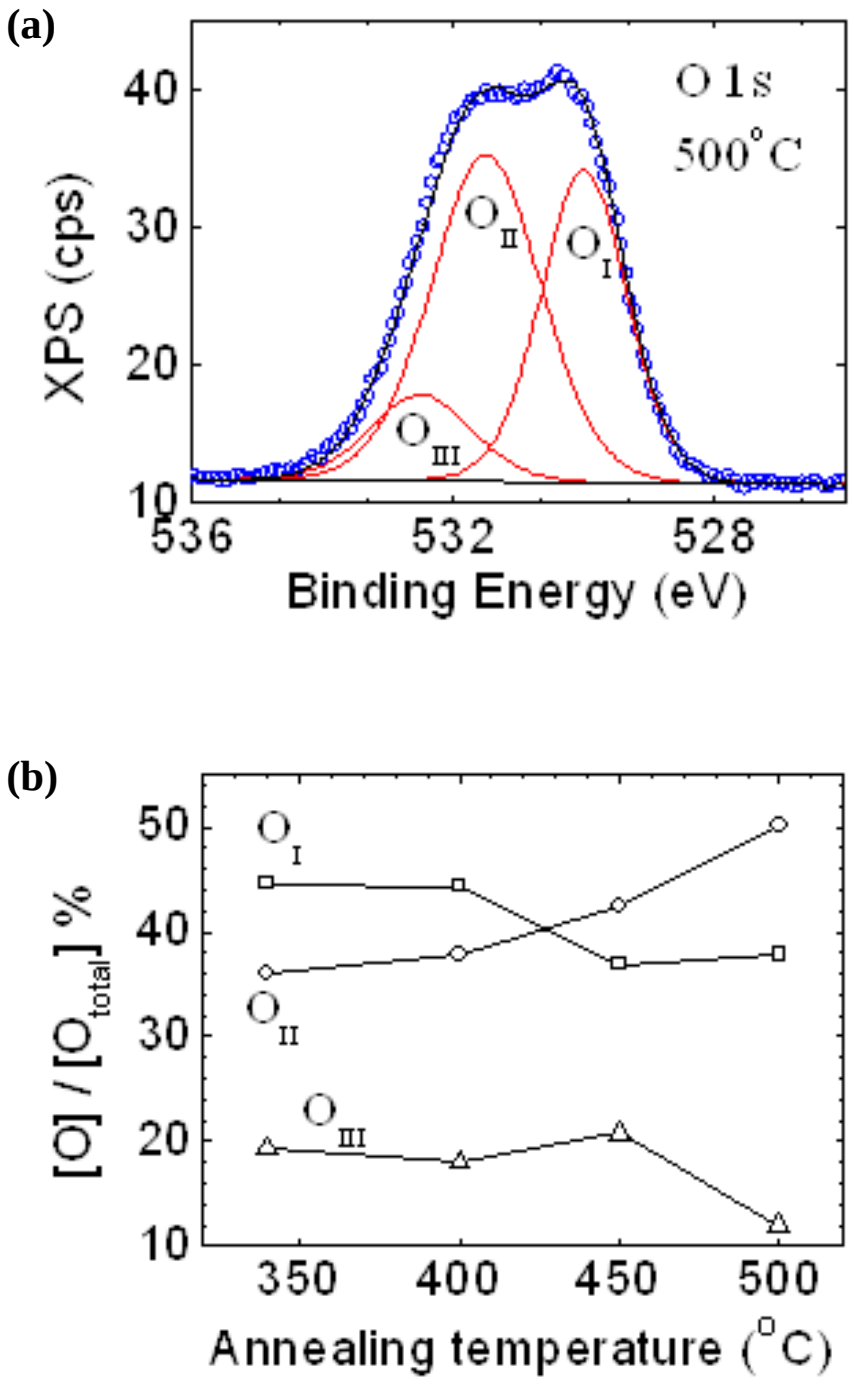

Figure 4.5 **(a)** XPS spectrum of O1s of the a-IGZO thin film annealed at 500 ℃ for 2 hours. **(b)** relative percentage ratios of different oxygen species changing with the annealing temperatures.

binding energy component O_{III} centred at 532.5 eV refers to the loosely bounded oxygen on the surface, which is mostly attributed to the hydrocarbon contamination, physically adsorbed oxygen and moisture. O_{III} obviously decreases from 20% to 12% at sufficiently high annealing temperature (>450 °C), suggesting substantial removal of surface hydrocarbon and physisorbed species. O_{II}, centred at 531.5 eV, is associated with O^{2-} ions that are in oxygen-deficient regions within the matrix of the a-IGZO, which supply free carriers to the a-IGZO films and results in free electron concentration in the a-IGZO channel. With the increase of annealing temperatures, $[O_{II}]/[O_{total}]$ gradually increases from 36 % (w.r.t. 15.6 atomic%) to 50% (w.r.t. 21.4 atomic%). It is believed that the enhancement of the mobility upon higher temperature annealing is attributed to the increase of the number of oxygen vacancies (O_{II}).

Figure 4.6 shows the TFT devices performance using a-IGZO active layers that deposited with precursor solutions containing different Ga ratios and the related electric properties are listed in **Table 4.2**. Ga ratio of 0.6 in precursor made the a-IGZO TFT hard to be turned off even the applied gate voltage increased to -60 V. Von decreases with Ga content, and V_{TH} becomes positive as the Ga ratio increased to 1.2. However, the mobility of a-IGZO layer with larger Ga content (x = 1.2) is also largely decreased to a value of 50 % lower (from 3.4 to 1.4. $cm^2V^{-1}s^{-1}$). The obtained results could be attributed to the nature of Ga element. Ga could offer stronger chemical bonds between metal and oxygen that reduces the concentration of free carriers and thus help reducing the Von [4]. However, too much Ga would also further reduce the oxygen deficiency thus decrease the mobility of a-IGZO films.

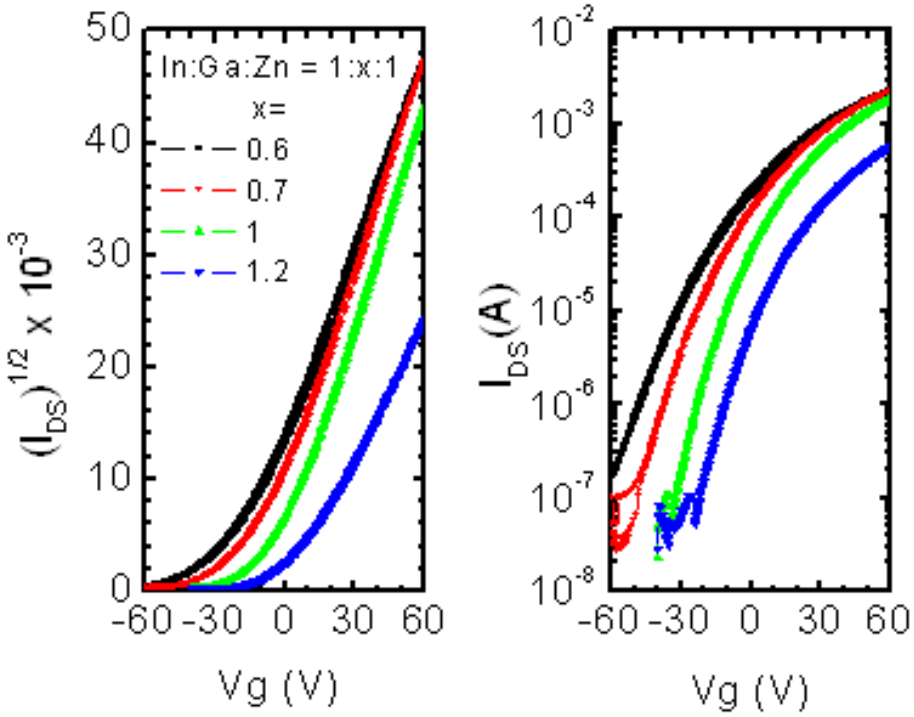

Figure 4.6 Drain current (I_{DS}) vs. gate voltage (Vg) transfer curves of TFTs with a-IGZO active layers prepared with different Ga ratios in precursor solutions (all of these films were annealed at 500 °C for 2 hours).

Table 4.2 The TFT device performance of the a-IGZO films prepared with different Ga ratios in precursor solutions.

Ga (x)	Mobility ($cm^2V^{-1}s^{-1}$)	V_{TH} (V)	Von (V)
0.6	3	-30	N/A
0.7	3.4	-17	-50
1	3.4	0	-32
1.2	1.4	7	-24

Conclusion

In brief, it has been demonstrated that MOD processed a-IGZO transistors have the basic characteristics of thin film transistors. The performance of a-IGZO TFT with the mobility of 3.4 $cm^2V^{-1}s^{-1}$ shows the newly developed approach promising. The operation mode of the a-IGZO is determined by the annealing temperatures. The spin-coating preparation of a-IGZO film is a rather simple process for transistor fabrication and therefore provides the possibility of low-cost manufacture of transparent TFTs with good performance.

REFERENCE

[1] K. Nomura, H. Ohta, A. Takagi, T. Kamiya, M. Hirano, and H. Hosono, Nature **432**, 488 (2004).

[2] H. Q. Chiang, J. F. Wager, R. L. Hoffman, J. Jeong, and D. A. Keszler, Appl. Phys. Lett. **86**, 013503 (2005).

[3] N. L. Dehuff, E. S. Kettenring, D. Hong, H. Q. Chiang, J. F. Wager, R. L. Hoffman, C.-H. Park, and D. A. Keszler, J. Appl. Phys. **97**, 064505 (2005).

[4] K. Nomura, A. Takagi, T. Kamiya, H. Ohta, M. Hirano, and H. Hosono, Jpn. J. Appl. Phys. **45**, 4303 (2006).

[5] H. Yabuta, M. Sano, K. Abe, T. Aiba, T. Den, H. Kumomi, K. Nomura, T. Kamiya, and H. Hosono, Appl. Phys. Lett. **89**, 112123 (2006).

[6] M. Kim, J. H. Jeong, H. J. Lee, T. K. Ahn, H. S. Shin, J.-S. Park, J. K. Jeong, Y.-G. Mo, and H. D. Kim, Appl. Phys. Lett. **90**, 212114 (2007).

[7] E. Fortunato, P. Barquinha, A. Pimentel, L. Pereira, G. Goncalves, and R. Martins, phys. stat. sol. (RRL) **1**, R34 (2007).

[8] D.-H. Lee, S.-Y. Han, G. S. Herman, and C.-H. Chang, J. Mater. Chem. **19**, 3135 (2009).

[9] T. Kamiya, and H. Hosono, NPG Asia Mater. **2**, 15 (2010).

[10] D. Kim, C. Y. Koo, K. Song, Y. Jeong, and, J. Moon, Appl. Phys. Lett. **95**, 103501 (2009).

[11] J. H. Lim, J. H. Shim, J. H. Choi, J. Joo, K. Park, H. Jeon, M. R. Moon, D. Jung, H. Kim, and H.-J. Lee, Appl. Phys. Lett. **95**, 012108 (2009).

[12] Y. H. Kim, M. K. Han, J. I. Han, and S. K. Park, IEEE Trans. Electron. Dev. **57**, 1009 (2010)

[13] S. J. Kim, G. H. Kim, D. L. Kim, D. N. Kim, and H. J. Kim, Phys. Status Solidi A **207**, 1668 (2010).

[14] Y. Wang, S. W. Liu, X. W. Sun, J. L. Zhao, G. K. L. Goh, Q. V. Vu, and H. Y. Yu, J. Sol-Gel Sci. Technol. **55**, 322 (2010).

[15] S. Jeong, Y.-G. Ha, J. Moon, A. Facchetti, and T. J. Marks, Adv. Mater. **22**, 1346 (2010).

[16] Y. Choi, G. H. Kim, W. H. Jeong, H. J. Kim, B. D. Chin, and J. W. Yu, Thin Solid Films **518**, 6249 (2010).

[17] C. Bae, D. Kim, S. Moon, T. Choi, Y. Kim, B. S. Kim, J. S. Lee, H. Shin, and J. Moon, ACS Appl. Mater. Interfaces **2**, 626 (2010).

[18] J. H. Choi, J. H. Shim, S. M. Hwang, J. Joo, K. Park, H. Kim, H.-J. Lee, J. H. Lim, M. R. Moon, and D. Jung, J. Korean Phys. Soc. **57**, 1836 (2010).

CHAPTER 5

OUTLOOK OF THE STUDY

In my doctorial study, the room temperature deposition of TiO_2 thin films that suitable for the fabrication of organic electronics has been proved. The room temperature deposited TiO_2 thin films could be prepared via liquid phase processes using nanoparticle dispersion. The well-dispersed TiO_2 nanoparticles were synthesized via hydrolysis reaction of $TiCl_4$ under low temperature, the average particle size of TiO_2 was around 2 nm, and the surface of nanoparticles was highly hydroxylated. To improve the performance of TiO_2/polymer hybrid electronic devices, post-annealing of TiO_2/polymer was applied to further remove the chemisorbed hydroxyl groups inside the TiO_2 layer and also to make the polymer diffuse into the bottom TiO_2 layer. Heterojunction of TiO_2 and polymer was formed with the post-annealing and the performance of TiO_2/F8BT copolymer hybrid LED was improved significantly due to the compact interconnection between these two materials and also the large interface area owing to the nanoscale combination.

From the results of my study, a novel process could be proposed that post-anneal the oxide/polymer bilayer to make a good heterojunction of these two materials, while the oxide layer has to be highly hydroxylated to reserve space for the later diffusion of polymer. The outlooks of this study are listed as below:

1. To deposit other kinds of metal oxide thin films on polymer substrates (e.g. PET) under low temperature using the nanoparticle aqueous dispersions, and then to test the performance of flexible oxide/polymer hybrid devices to verify

the feasibility of this low temperature process for the fabrication of flexible electronics.

2. To prepare oxide/polymer bilayer with good heterojunction by process developed in this study. Besides TiO_2, oxides like ZnO should be applied to examine their potential usages in oxide/polymer hybrid devices.
3. To synthesize oxide nanoparticles by methods other than hydrolysis reaction used here, try to change the surface conditions of nanoparticles or to reduce the impurities to further improve the performance of hybrid devices.

The results of study to deposit a-IGZO films via MOD solution process prove that the newly developed process using acetylacetonates as precursors is promising to easily fabricate transparent TFT in large scale under moderate temperatures. The outlooks of this part of study are:

1. To modify the MOD process by replacing the acetylacetonates with other compounds, e.g. acetates or ethoxides to change the decomposition behavior of precursors and then to improve the control of element composition.
2. To reduce the V_{TH} while also increasing the mobility by doping metal ions other than In, Ga and Zn, i.e. to examine the effect of exotic dopants.

The results of this study show that as long as we keep working, the advanced electronics (flexible, transparent, and large area) fabricated by low-cost and energy-saving processes are coming soon.